

RAPIDLY ROTATING ULTRACOLD ATOMS IN HARMONIC TRAPS

A THESIS SUBMITTED TO
THE GRADUATE SCHOOL OF NATURAL AND APPLIED SCIENCES
OF
MIDDLE EAST TECHNICAL UNIVERSITY

BY

NADER GHAZANFARI

IN PARTIAL FULFILLMENT OF THE REQUIREMENTS
FOR
THE DEGREE OF PHILOSOPHY OF DOCTORATE
IN
PHYSICS

JUNE 2011

Approval of the thesis:

RAPIDLY ROTATING ULTRACOLD ATOMS IN HARMONIC TRAPS

submitted by **NADER GHAZANFARI** in partial fulfillment of the requirements for the degree of **Philosophy of Doctorate in Physics Department, Middle East Technical University** by,

Prof. Dr. Canan Özgen
Dean, Graduate School of **Natural and Applied Sciences**

Prof. Dr. Sinan Bilikmen
Head of Department, **Physics**

Prof. Dr. Altuğ Özpineci
Supervisor, **Physics Department, METU**

Assoc. Prof. Dr. Mehmet Özgür Oktel
Co-supervisor, **Physics Department, Bilkent University**

Examining Committee Members:

Assoc. Prof. Dr. Afif Sıddıki
Physics Department, Istanbul University

Prof. Dr. Altuğ Özpineci
Physics Department, METU

Assoc. Prof. Dr. Özgür Esat Müstecaplıoğlu
Physics Department, Koç University

Assoc. Prof. Dr. Sadi Turgut
Physics Department, METU

Assist. Prof. Dr. Hande Toffoli
Physics Department, METU

Date:

I hereby declare that all information in this document has been obtained and presented in accordance with academic rules and ethical conduct. I also declare that, as required by these rules and conduct, I have fully cited and referenced all material and results that are not original to this work.

Name, Last Name: NADER GHAZANFARI

Signature :

ABSTRACT

RAPIDLY ROTATING ULTRACOLD ATOMS IN HARMONIC TRAPS

Ghazanfari, Nader

Ph.D., Department of Physics

Supervisor : Prof. Dr. Altuğ Özpineci

Co-Supervisor : Assoc. Prof. Dr. Mehmet Özgür Oktel

June 2011, 67 pages

In this study we investigate the properties of trapped atoms subjected to rapid rotations. The study is divided into two distinct parts, one for fermions, another for bosons. In the case of the degenerate Fermi gas we explore the density structure of non-interacting cold atoms when they are rotated rapidly. On the other hand, for rapidly rotating two component Bose condensate, we search for new lattice structures in the presence of contact and dipolar interactions.

First, the density structure of Fermi gases in a rotating trap is investigated. We focus on the anisotropic trap case, in which two distinct regimes, two and one dimensional regimes, depending on rotation frequency and anisotropy are observed. Two regimes can be illustrated by a simple description of maximum number of states between two Landau levels, which is strongly related to the dimensionality of the system. The regimes are separated from each other by a minimum point in this description. For small anisotropy values the density profiles show a step structure where each step is demonstrated by an elliptical plateau. Each plateau represents a Landau level with a constant density. The local density approximation describes the two dimensional regime with a perfect similarity in the structure of fermion density. The case for

one dimensional regime is a little different from the two dimensional case. For large anisotropy values the Friedel oscillation is the dominant aspect of the density profiles. The density profiles show gaussian structure along the direction of strong trapping, and a semicircular form with prominent oscillations along the weak confining direction. Again, the system is nicely described by local density approximation in this regime. A smooth crossover between two regimes is observed, with a switching from a step structure profile to a soft edge transition with Friedel oscillations. At finite temperatures, the step structures are smeared out in two dimension. In one dimensional regime the Friedel oscillations are cleaned as soon as the temperature is turned on.

The second part of the study is devoted to the investigation of different lattice structures in two component Bose condensates subjected to very fast rotation, this time in the presence of interactions. We explore the existence of new vortex lattice structures for dipolar two component condensates scanning a wide range of interaction strengths. We introduce a phase diagram as a function of intra and inter-component interactions showing different type of vortex lattice structures. New types of lattice structures, overlapped square and overlapped rectangular, emerge as a result of dipolar interactions and s-wave interaction for a two component condensate. The region where the attractive inter-component interactions dominate the repulsive interactions, the overlapped lattices are formed. The intra-component interactions, which defines the behavior of each component inside, result in different type of lattices by changing the strength of interactions. Two different limits of phase diagram reproduce the results of ordinary two component and dipolar one component Bose condensates. The results of calculation are in agreement with the results of previous studies for two regimes.

Keywords: Degenerate Fermi gas, Bose-Einstein condensate, rapidly rotating, fermion density, vortex lattice

ÖZ

HARMONİK TUZAKLARDA HIZLI DÖNEN ULTRASOĞUK ATOMLAR

Ghazanfari, Nader

Doktora, Fizik Bölümü

Tez Yöneticisi : Prof. Dr. Altuğ Özpineci

Ortak Tez Yöneticisi : Assoc. Prof. Dr. Mehmet Özgür Oktel

Haziran 2011, 67 sayfa

Bu çalışmada hızı dönmeye tabi tutulan harmonik tuzaklardaki atomların özellikleri incelenmektedir. Çalışma fermiyonlar ve bosonlardan oluşan iki farklı bölüme ayrılmıştır. Dejenere Fermi gazlarda etkileşmeyen ultrasoğuk atomların yoğunluk profilleri hızlı dönme altında incelenmiştir. Hızlı dönen iki bileşenli Bose-Einstein yoğunlaşmasında ise yeni girdap örgüleri kontakt ve dipol etkileşimleri altında araştırılmıştır.

İlk önce, Harmonik tuzaklarda dönen Fermi gazların yoğunluk profilleri incelenmiştir. Çalışmada eşyönsüz tuzaklar üzerine yoğunlaşıldı. Bu durumda eşyönsüzlükle dönme hızına bağlı olarak iki farklı rejim gözlenmekte. Bu rejimler iki ve bir boyutlu rejimler olarak görülmektedir. Bu iki rejim ardışık olan iki Landau düzeyinin arasındaki durumların maksimum sayısını tanımlayan parametre ile açıklanabilir. Bu parametre sistemin boyutu ile ilişkili. İki rejim söz konusu parametrenin minimum değerinde buluşmaktadır. Küçük eşyönsüzlükler için yoğunluk profilleri basamaklı yapı ortaya koymaktadır. Her basamak ise elips şeklinde olan sabit yoğunluktan oluşan düzlüklerden ibarettir. Lokal yoğunluk yaklaşımı iki boyutlu rejimi kusursuz benzerlikle açıklamaktadır. Bir boyutlu rejim, iki boyutlu rejime göre önemli farklılıklar ortaya koymaktadır. Büyük eşyönsüzlüklerde Friedel salınımları yoğunluk profil-

lerinin baskın yönünü oluşturmaktadır. Yoğunluk profilleri güçlü tuzaklama yönünde gausiyen bir yapıya sahiptirler. Diğer yönde ise, yani zayıf tuzaklama yönünde, Friedel salınımları belirgin olduğu yarı daireseller görünmektedir. Bu rejimde de lokal yoğunluk yaklaşımı sistemin yoğunluğunu numerik hesaplarla uyumlu biçimde açıklamaktadır. İki rejim arasında düzgün geçiş gözlenmektedir. Yüksek sıcaklıklarda iki boyuttaki basamaklı yapı ortadan kalmakta, bir boyatta ise Friedel salınımları ortadan kalkmıştır.

Çalışmanın ikinci bölümünde hızlı dönmeye tabi tutulmuş iki bileşenli Bose-Einstein yoğunlaşmasında farklı girdap örgü yapılarının oluşumlarını incelenmiştir. Burada bir diğer önemli konu ise etkileşimlerin var olmasıdır. Geniş etkileşim aralıkları taranarak iki bileşenli yoğunlaşmada ortaya çıkan girdap örgüleri tespit edilmiştir. Sonuç olarak kontak ve dipol etkileşimlerinin sunduğu yeni örgü yapıları bulunmuştur. Etkileşimlerin doğası, yani etkileşimlerin çekici veya itici olmaları, bu yeni örgülerin oluşumunda önemli rol oynamaktadır. Bu gazların ortaya koyduğu genel örgü yapıları ise bir faz diagramında sunulmuştur. Faz diagramının iki limitinin sonuçları, dipol etkileşimine sahip olan tek bileşenli Bose yoğunlaşması ve dipol etkileşimi olmayan iki bileşenli Bose yoğunlaşması olmak üzere, daha önceki çalışmalarla birebir örtüşmektedir.

Anahtar Kelimeler: dejenere Fermi gazı, Bose-Einstein yoğunlaşması, hızlı dönen, fermiyon yoğunluğu, girdap örgüleri

To my mother

ACKNOWLEDGMENTS

I would like to express my deep and sincere gratitude to Assoc. Prof. Dr. Mehmet Özgür Oktel for his guidance, support, and encouragement throughout my Ph.D. studies. I would also like to send my sincere gratefulness to Prof. Dr. Altuğ Özpineci for his endless helps during my Ph.D. studies.

I would like to thank my dear friends Onur Umucalılar, Ahmet Keleş, and Levent Subaşı for useful discussions through carrying out this research. I also want to present my thanks to Tahsin Çağrı Şişman and other friends from Muhabbet-i Fizikiyye for enjoyable discussions about physics.

I thank my dear friends Yakup Pekön, Çağan Aksak, Kıvılcım Vural, Sibel Sayın, Taylan Takan, İnanç Kanık, Nazan Kara, Gülnur Doğan, Davut Turan, and Sanay Rashedi for their companionship.

My special thanks goes to my homemate, and best friend Chiko the Great, who always wakes me up early morning to open the window for him to go out and watch birds.

I especially thank Oya Aktaş for her love, patience and understanding.

I am grateful to my family for their endless love, and moral support through all these years.

Finally, I acknowledge the financial support from TUBITAK, The Scientific and Technological Research Council of Turkey.

TABLE OF CONTENTS

ABSTRACT	iv
ÖZ	vi
ACKNOWLEDGMENTS	ix
TABLE OF CONTENTS	x
LIST OF FIGURES	xii
CHAPTERS	
1 INTRODUCTION	1
1.1 Interactions in dilute ultracold atoms	3
1.2 Theory of weakly interacting Bose gases	5
1.3 Rotating Ultracold atoms	6
2 RAPIDLY ROTATING FERMIONS IN HARMONIC TRAPS	10
2.1 Rapidly rotating Fermions: isotropic case	11
2.2 Rapidly rotating fermions: anisotropic case	17
2.2.1 One and two dimensional regimes	23
2.2.2 Density Profiles	25
2.2.3 Temperature effects	34
3 VORTEX LATTICES OF RAPIDLY ROTATING BOSE-EINSTEIN CONDENSATES	36
3.1 Mean field quantum Hall regime	38
3.2 Vortex lattices of dipolar two component Bose-Einstein con- densates	40
3.2.1 Vortex pattern	45
4 SUMMARY AND CONCLUSION	52
REFERENCES	55

APPENDICES

A	Canonical transformation in quantum mechanics	60
B	Wavefunctions of higher Landau levels for a particle in a rotating anisotropic harmonic trap	64
VITA	65

LIST OF FIGURES

FIGURES

Figure 1.1 (a) The condensate is irrotational when the phase of the condensate wavefunction has no singularity. (b) The rotation can be defined when there is hole in the phase of the condensate wavefunction.	8
Figure 1.2 Vortex lattice	9
Figure 2.1 Energy vs. number of states in each Landau levels. l is the highest number of states within LL's before the next LL is excited.	13
Figure 2.2 (a) Density profile for fermions filling three Landau levels. The Landau levels are represented by a disk like structure. (b) Density profile for fermions occupying the lowest Landau level.	14
Figure 2.3 Density profile for fermions at different temperatures and at $\Omega/\omega = 0.99$. The layered aspect of the profile is eliminated by temperature. . . .	16
Figure 2.4 Density of fifth wavefunction at different anisotropies, and fixed rotation frequency, $\Omega/\omega_x = 0.99$. Increasing the anisotropy breaks up the fifth order zeros in the origin to row of zeros along the weak trapping direction.	22
Figure 2.5 Solid line shows the behavior of l , maximum number of states within two LL's as a function of the anisotropy of the system ω_y/ω_x . Dashed lines are the asymptotic results for one and two dimensional limits. Here $\omega_{yc} = (1 + 4\Omega^2/\omega_x^2)^{1/2}$ is the critical anisotropy where l is minimum. The minimum number of states is given by $l_c = (\frac{8}{1-\Omega/\omega_x})^{1/2}$	24

Figure 2.6 Density profiles for fermions at different anisotropy values of the system and fixed number of the particles $N=1000$, and fixed rotation frequency $\Omega/\omega_x = 0.999$. The Friedel oscillations are observed in density profiles of anisotropic cases. The number of LL's that fermions fill at each anisotropy can also be determined by counting the number of plateaus in the density profiles. 26

Figure 2.7 Density profiles of fermions at different anisotropy values of the system and fixed number of the particles $N=200$, and fixed rotation parameter $\Omega/\omega_x = 0.9999$, when all the fermions are settled at the LLL. The Friedel oscillations are also observed for density profiles of anisotropic cases. 28

Figure 2.8 (a) Density for $N=200$ fermions at $\Omega/\omega_x = 0.9999$, and $\omega_y/\omega_x = 1.5$. (b) Density for $N=200$ fermions at $\Omega/\omega_x = 0.9999$, and $\omega_y/\omega_x = 5$. The insets in both figures highlight the Friedel oscillation in density profiles of the fermions. 31

Figure 2.9 (a) Density of $N=550$ fermions obtained by direct numerical calculations (solid line), and two dimensional LDA (dashed line) at $\Omega/\omega_x = 0.999$, and $\omega_y/\omega_x = 1.05$. (b) Density of $N=200$ fermions obtained by direct numerical calculations (solid line), and one dimensional LDA (dashed line) at $\Omega/\omega_x = 0.9999$, and $\omega_y/\omega_x = 3.5$ 33

Figure 2.10 (a) Density profile for fermions at different temperatures and at $\Omega/\omega_x = 0.99$, and $\omega_y/\Omega_x = 3.5$. (b) Density profile for fermions at different temperatures and at $\Omega/\omega_x = 0.99$, and $\omega_y/\Omega_x = 1.01$. The oscillations (a) and the layered aspect of the profiles (b) are eliminated by temperature. Here $\beta = \frac{\hbar\omega_x}{k_b T}$ is the normalized inverse temperature. 35

Figure 3.1 Dipole-dipole interaction. 41

Figure 3.2	Phase diagram showing lattice structures for different values of interaction terms α , and β . Here, C corresponds to collapse region, and IR, IS, IO, IT, OR, OT, and OS stand for interlaced rectangular, interlaced square, interlaced oblique, interlaced triangle, overlapped rectangular, overlapped triangle, and overlapped square, respectively. The inset figure indicates the region for overlapped square lattices, a new type of lattice structure for rotating Bose condensates.	46
Figure 3.3	The parameters indicating the type of lattice structures as a function of interaction terms α , and β . The phase diagram is reduced to different regimes: (a) The limit for ordinary two component condensate. (b) The limit for dipolar single component condensate. Here τ and, θ are the lattice parameters and define the lattice structure, and a , indicates the displacement of the lattice structures of one species with respect to another species.	48
Figure 3.4	Lattice structures for dipolar two component condensates. Black and gray dots corresponds to vortices of two condensates.	50

CHAPTER 1

INTRODUCTION

Dramatic progresses in laser-based techniques in cooling and trapping of alkali atoms started a new era in condensed matter physics, both theoretically and experimentally. Decades after the first theoretical demonstration of Bose-Einstein condensation (BEC) [1, 2, 3], the experimental observations of the macroscopic occupation of a single particle state were carried out [4, 5, 6]. The achievement was not only the manifestation of an interesting phenomena, but also provided a great opportunity to make bridges to study the nature of some other exotic many body systems, such as superfluidity. Although the early years of the field were devoted to investigate the important properties of BEC and its consequences, the theoretical and experimental efforts were accelerated to study the fermionic nature of ultracold atoms, as soon as the difficulties in cooling of Fermi gases due to the Pauli exclusion principle were overcome.

Interactions play a very important role in determining the properties of ultracold atoms. Dynamics and stability of trapped atoms as well as ground states properties of these quantum gases are highly influenced by the strength and quality of the interactions [7]. The systematic study of the nature of such many body systems, with the interaction present needs a powerful theoretical tool. The need for a fine theoretical description of ultracold atoms with a good agreement with the experimental results was met by the Gross-Pitaevskii equation (GPE) [8, 9, 10]. This theory gives a zero-temperature description of atomic Bose gases when conditions for its validity are satisfied [7, 11]. The existence of other interactions like the dipole-dipole interaction enriches the topics of the field to go even beyond, and investigate the properties of long range interactions in more detail.

Ultracold atoms have some important features that make the system a rich subject of study. One of the most significant properties of the cold atoms is the unprecedented degrees of control over some vital parameters, such as interactions, and dimensionality, which serves physicists a clean, and flexible environment to simulate various many-body systems ranging from solid crystals to relativistic particles [12]. Thanks to the observations of Feshbach resonances in ultracold atoms [13, 14, 15], the tuning of the interactions, either quantitatively or qualitatively is carried out during the experiments, in a relatively easy manner. Such an ability provide the chance to go from attractive to repulsive interactions, even create strongly correlated systems. On the other hand, optical potentials provided the possibility of generating different trapping geometries and its combination with Feshbach resonances results in realizing very interesting systems or quantum phenomena [16, 17, 18]. The theoretical suggestions [19, 20, 21] and afterward observation of a Tonks-Girardeau gas [22, 23], and the quantum transition from superfluid phase to Mott-insulating state [24] are examples of cooperations discussed above.

Another important feature of ultracold atoms is their response to external potentials. The rotation of ultracold atoms, especially Bose gases was a matter of interest from early days of the BEC era. Theoretically, the response of superfluids to the rotations is widely studied and well known since the first predictions of quantized vortices when exceeding a certain critical velocity [25, 26]. The attempts to observe the vortices in atomic condensates succeeded only a few years later after observations of BEC [27, 28, 29]. The equivalence of the Coriolis force and the Lorentz force when appearing in a Hamiltonian also opened a new page in the field of atomic gases. The exploration of quantum Hall physics in rapidly rotating ultracold atoms started with first signs of connection between two fields [30, 31]. In order to have a better understanding of the physics of rapidly rotating ultracold atoms for both bosons and fermions along with the interactions, we review the basic ideas of ultracold atoms, especially those who help us follow the main ideas discussed in the next chapters.

1.1 Interactions in dilute ultracold atoms

Ultracold atoms are dilute gases, i.e. the interatomic separation, determined by average density of the gas, is much larger than the range of interatomic interactions. Quantitatively speaking, the density of ultracold atoms is about $10^{12} - 10^{15}$ particle per cm^3 , which gives an average interparticle spacing of $0.1 - 1 \mu m$. This particle separation is at least one order of magnitude larger than the atom-atom interaction length scales. The dilute nature of trapped atoms allows to consider only the binary collisions and neglect three or more particle interactions. Moreover, the temperature is sufficiently low, then the de Broglie wavelength is so large that the specific nature or physical details of finer interatomic interactions are not important anymore. Therefore the low energy two-body scattering is sufficient to describe the system and one can express the interaction potential in terms of a single parameter, the scattering length [7, 11, 32, 33]. In order to introduce the scattering length it would be better to have a short review of basic aspects of the scattering theory.

We consider the scattering of two atoms and aim to solve the Schrodinger equation to obtain the wavefunctions. Since we deal with the a two-particle problem, we make a transformation to the center of mass coordinates. The wavefunction for the relative motion of the atoms contains the information about the scattering. One can find in most text books of quantum mechanics that the wavefunction can be written as [34]

$$\begin{aligned}\psi &= \frac{1}{(2\pi)^{3/2}} \left[e^{i\mathbf{k}\cdot\mathbf{r}} + \frac{e^{ikr}}{r} f(\mathbf{k}, \mathbf{k}') \right] \\ &= \frac{1}{(2\pi)^{3/2}} \left[e^{i\mathbf{k}\cdot\mathbf{r}} + \frac{e^{ikr}}{r} f(\theta) \right],\end{aligned}\tag{1.1}$$

which reduces to the plane wave solution when there is no scattering. Here $f(\mathbf{k}, \mathbf{k}')$ is the scattering amplitude with \mathbf{k} , and \mathbf{k}' are the wave vectors for incoming and scattered waves, respectively, both with magnitude k . Note that θ is the angle between two wave vectors. To determine the overall effect of scattering one needs to obtain the cross section $\sigma(E)$, which is calculated from the differential cross section

$$\frac{d\sigma}{d\Omega} = |f(\mathbf{k}, \mathbf{k}')|^2.\tag{1.2}$$

At low energies the s-wave scattering is the dominant part, and one can neglect the other contributions to the scattering [32]. Such an approximation leads us to write the

cross section in terms of s-wave scattering length a as

$$\sigma(E) = 4\pi a^2. \quad (1.3)$$

We discussed the problem of scattering for distinguishable particles. To be more specific in calculating the scattering cross section we may add the effects of indistinguishability. Alkali atoms have different internal states arising from couplings of electronic and nuclear spins, called atomic hyperfine states. Let us suppose that we have two identical particles, i.e. atoms occupying the same hyperfine states. Then we have to symmetrize or antisymmetrize the wavefunction due to the total spin of atoms, when they are bosons or fermions. The differential cross section considering the symmetrized wavefunction becomes

$$\frac{d\sigma}{d\Omega} = |f(\theta) \pm f(\pi - \theta)|^2, \quad (1.4)$$

the plus and minus signs refer to bosons and fermions, respectively. Again by integrating the differential cross section over all final directions the total cross section is obtained as

$$\sigma = \begin{cases} 8\pi a^2 & \text{for bosons} \\ 0 & \text{for fermions} \end{cases} \quad (1.5)$$

The result shows that two polarized fermions can be considered to be non-interacting. However, the scattering is present when fermionic atoms occupy different hyperfine states.

We discussed above that the diluteness of ultracold atoms allows one to ignore the actual nature of interactions and replace the interaction with an effective potential which gives the correct s-wave scattering length. A good candidate to such potential may have the form of contact interaction which is proportional to scattering length

$$U_{eff}(\mathbf{r}) = \frac{2\pi a \hbar^2}{M_r} \delta(\mathbf{r}). \quad (1.6)$$

An important subject related to the scattering of two atoms is that the strength of the interaction can be altered via a phenomenon called Feshbach resonances [35]. Tuning the strength of the interaction in this method specifically is controlling the strength of s-wave scattering length and its sign [13, 14, 15], which determines the nature of interaction, whether it is repulsive or attractive. The use of magnetically tunable

Feshbach resonances not only makes the study of the properties of the condensates easier [36, 37, 38, 39], but also provides the chance of going to the state of strongly interacting Fermi systems or study the nature of other physics [23, 24, 40, 41].

1.2 Theory of weakly interacting Bose gases

Sometimes it is difficult to handle a many-body system when considering a realistic model. However, it can be approached by relatively easy approximate methods. The symmetries with other features of the systems provide a ground to apply approximations, giving results in good agreement with the experiments. One of such approximations is the Gross-Pitaevskii theory of condensed Bose gases. Roughly speaking the Gross-Pitaevskii theory is the Hartree-Fock approximation at $T = 0$ for a BEC system. This theory treats the interactions in a mean field regime, which avoids the heavy calculations of solving the many-body Schrodinger equation. We first derive the Gross-Pitaevskii equation starting with the many-body Hamiltonian describing a system of N interacting identical bosonic atoms in a trapping potential, $V_{ext}(\mathbf{r})$

$$H = \int d\mathbf{r} \left[\frac{\hbar^2}{2M} |\nabla \Psi(\mathbf{r})|^2 + V_{ext}(\mathbf{r}) |\Psi(\mathbf{r})|^2 \right] + \int d\mathbf{r} d\mathbf{r}' \Psi^\dagger(\mathbf{r}) \Psi^\dagger(\mathbf{r}') V(\mathbf{r} - \mathbf{r}') \Psi(\mathbf{r}') \Psi(\mathbf{r}). \quad (1.7)$$

Where $\Psi(\mathbf{r})$, and $\Psi^\dagger(\mathbf{r})$ are the field operators (annihilation and creation, respectively) obeying bosonic commutation relations, and $V(\mathbf{r} - \mathbf{r}')$ is the interaction potential between two atoms. The Hamiltonian itself gives the properties of the system but needs a great amount of numerical calculations [42] even for moderately large number of particles. However, in the case of atomic condensation one can obtain an equation from time evolution of field operator, which is much more convenient for calculations. The Heisenberg equation of motion gives the time evolution for field operator $\Psi(\mathbf{r})$ as

$$\begin{aligned} i\hbar \frac{\partial}{\partial t} \Psi(\mathbf{r}, t) &= [\Psi(\mathbf{r}, t), H] \\ &= -\frac{\hbar^2}{2M} \nabla^2 \Psi(\mathbf{r}, t) + V_{ext}(\mathbf{r}) \Psi(\mathbf{r}, t) \\ &+ \int d\mathbf{r}' \Psi^\dagger(\mathbf{r}', t) V(\mathbf{r} - \mathbf{r}') \Psi(\mathbf{r}', t) \Psi(\mathbf{r}, t). \end{aligned} \quad (1.8)$$

For the case of dilute atomic gases we write an effective potential giving the same characteristic length of the real potential, in the previous section (see Eq. (1.6)). Also for a condensed Bose gas with a large number of atoms, one can replace the field operator Ψ with the classical field function ψ . With these replacements, the useful equation of Gross-Pitaevskii can be established [11, 7, 32, 43]

$$i\hbar \frac{\partial}{\partial t} \psi(\mathbf{r}, t) = -\frac{\hbar^2}{2M} \nabla^2 \psi(\mathbf{r}, t) + V_{ext}(\mathbf{r})\psi(\mathbf{r}, t) + g|\psi(\mathbf{r}, t)|^2 \psi(\mathbf{r}, t) \quad (1.9)$$

Here $g = 4\pi\hbar^2 a/M$ is the coupling constant related to the scattering for two identical atoms. The equation was derived by Gross [8, 9] and Pitaevskii [10], independently to investigate the properties of weakly interacting non-uniform Bose gases at low temperatures.

The GPE has been used widely to study the condensate state both analytically and numerically ensuring a good agreement with the experimental results. It is a great theoretical tool to investigate the dynamics of condensates such as elementary excitations, collective oscillations, and solitary waves [32]. Moreover, the static properties of the system can be investigated using the time-independent GPE

$$-\frac{\hbar^2}{2M} \nabla^2 \psi(\mathbf{r}) + V_{ext}(\mathbf{r})\psi(\mathbf{r}) + g|\psi(\mathbf{r})|^2 \psi(\mathbf{r}) = \mu\psi(\mathbf{r}). \quad (1.10)$$

where μ is the chemical potential.

The trap potentials in the experiments of ultracold atoms could be considered as harmonic potentials when approaching the problem theoretically. With the known external potential, ground state properties of trapped bosons can be obtained either numerically or analytically from Eq. (1.10). The analytical solutions could be obtained with different methods such as variational methods, or Thomas-Fermi approximation [44, 45, 46], however, its numerical solution are relatively easy to obtain [47, 48, 49].

1.3 Rotating Ultracold atoms

The response of the ultracold atoms to the rotation has been a matter of interest since the first observations of BEC. The rotation of the superfluids gives rise to the existence of quantized vortices well known for more than half a century [25, 26]. The same

property was predicted for Bose-Einstein condensates as they exhibit the same constrained motions under rotation. The observation of vortices in atomic Bose-Einstein condensates [50, 51, 52] is the most important achievement after the experimental manifestation of BEC itself. Thus, let us first start with the quantum hydrodynamics of the condensate in the presence of rotations. The most important property of a condensate is that a macroscopic wavefunction can describe the condensed Bose gas, which is written as

$$\begin{aligned}\Psi(\mathbf{r}, t) &= |\Psi(\mathbf{r}, t)|e^{iS(\mathbf{r}, t)} \\ &= \sqrt{n(\mathbf{r}, t)}e^{iS(\mathbf{r}, t)},\end{aligned}\tag{1.11}$$

where n is the density of the condensate, and S is the overall phase of the condensate. The velocity field can be obtained from the current density defined from GPE (1.9)

$$\begin{aligned}\mathbf{j} &= n(\mathbf{r}, t)\mathbf{v}(\mathbf{r}, t) \\ &= \frac{\hbar}{2Mi} [\Psi^* \nabla \Psi - \Psi \nabla \Psi^*]\end{aligned}\tag{1.12}$$

In the case of a classical fluid the velocity field rotating with the frequency Ω obeys the relation for rigid body rotation

$$\mathbf{v}_c = \boldsymbol{\Omega} \times \mathbf{r},\tag{1.13}$$

for which the vorticity is uniform, i.e.

$$\nabla \times \mathbf{v}_c = 2\boldsymbol{\Omega}\tag{1.14}$$

However, this is not the case for a condensate, since the velocity field is proportional to the gradient of the scalar field $S(\mathbf{r}, t)$

$$\mathbf{v} = \frac{\hbar}{M} \nabla S(\mathbf{r}, t).\tag{1.15}$$

Apparently the velocity field is irrotational, in other words the condensate vorticity vanishes

$$\nabla \times \mathbf{v} = \frac{\hbar}{M} \nabla \times \nabla S(\mathbf{r}, t) = 0.\tag{1.16}$$

Stokes's theorem implies that for any close path in a simply connected geometry one can write

$$\int \nabla \times \mathbf{v} \cdot d\mathbf{a} = \oint \mathbf{v} \cdot d\mathbf{l} = 0.\tag{1.17}$$

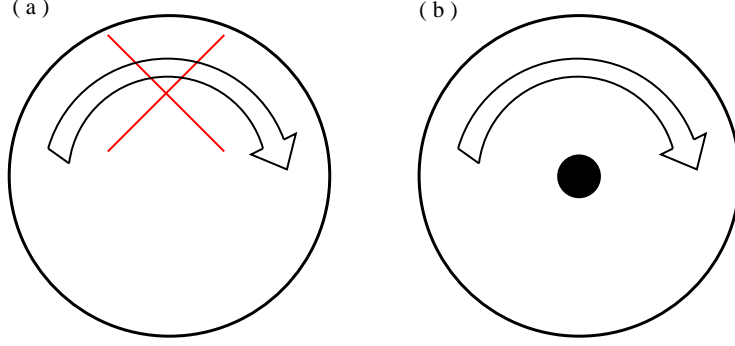


Figure 1.1: (a) The condensate is irrotational when the phase of the condensate wavefunction has no singularity. (b) The rotation can be defined when there is hole in the phase of the condensate wavefunction.

However, for a function which is not simply connected the rotation happens in a different manner (see figure 1.1). Let us assume that the phase has a hole. Since the condensate wavefunction must be single valued, the change in the phase around any closed path must be an integral multiple of 2π ,

$$\Delta\phi = \oint d\mathbf{l} \cdot \nabla S(\mathbf{r}, t) = 2\pi l \quad (1.18)$$

where l is an integer number. Again, defining the circulation

$$\oint \mathbf{v} \cdot d\mathbf{l} = l \frac{h}{M}, \quad (1.19)$$

reveals that the circulation is quantized in units of h/M , called the vortex line. Physically speaking, a rotating condensed Bose gas lowers its energy by nucleating vortices. One can create a large number of vortices by increasing the rotation velocity Ω [11, 7, 32, 53, 54] (see figure 1.2, for example). Along with the investigations of quantized vortices in rotating atomic condensates which is an exciting phenomenon, the hopes to reach a state of strongly correlated system in dilute atomic gases become more realistic with the existence of traps especially when they are rotating. The rotation increases the effect of interactions when the rotation frequency approaches a limit, the frequency of the trap [55, 56, 57]. With the Feshbach resonances the interaction between atoms can also be controlled quantitatively and qualitatively to even go beyond the usual interaction ranges to obtain the novel states of strongly interacting systems, which opens the horizons of studying the physics of quantum Hall effect in

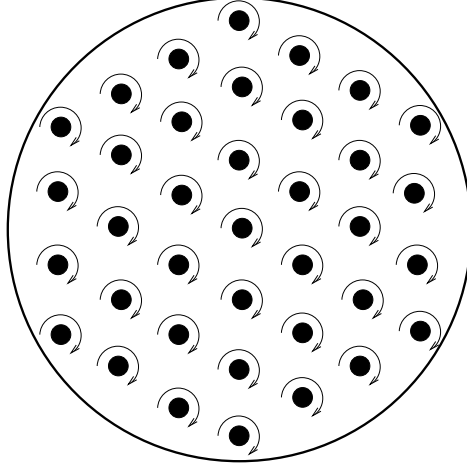


Figure 1.2: Vortex lattice

a system of particles different from original matter of subject [57, 58, 59]. The equivalence of the Coriolis force to the Lorentz force when appearing in the Hamiltonian is the first clue to construct a connection between two completely different systems [30, 31]. The single particle Hamiltonian of an ultracold atom trapped in rotating harmonic potential in the rotating frame

$$\begin{aligned}
 H &= \frac{P^2}{2M} + \frac{1}{2}M\omega^2 r^2 - L_z \Omega \\
 &= \frac{1}{2M} (P - M\mathbf{\Omega} \times \mathbf{r})^2 + \frac{1}{2}M(\omega^2 - \Omega^2) r^2.
 \end{aligned} \tag{1.20}$$

Here M is the mass of the particle, ω is the trap frequency, and L_z is the angular momentum in the z direction. One can define an effective vector potential, $\mathbf{A} = \frac{M}{q}\mathbf{\Omega} \times \mathbf{r}$ to show the explicit equivalence of two systems.

In the case of a rapidly rotating condensate, the regime of high vortex density when the number of vortices is larger than number of atoms [57], the bosonic analogy of a fractional quantum hall effect in semiconductors can be constructed [53]. Although the s -wave interaction is absent for identical particles in the case of atomic Fermi gases, the tunable p -wave interaction or dipole-dipole interactions also makes it possible to create the state of strongly correlated system with these atoms [58].

CHAPTER 2

RAPIDLY ROTATING FERMIONS IN HARMONIC TRAPS

The cooling of Fermi gases with alkali atoms is difficult since the identical fermions are non-interacting. However, a two component Fermi gas, two atoms occupying different hyperfine states, can experience s-wave interaction between atoms. Another possibility is a mixture of Bose-Fermi gases which ensure the existence of interactions. The two methods were successfully implemented and the Fermi gases were cooled below the Fermi temperature [60, 61, 62, 63, 64, 65]. The observation of the degenerate Fermi gas provides an important tool to observe another exotic phenomenon of Cooper pairs in BCS theory of superconductivity [66, 67], or study the crossover between BCS and BEC regimes [12].

Moreover, the properties of degenerate Fermi gases under rotation could also be interesting. For a two-dimensional electron gas subjected to a strong magnetic field, the energy spectrum reveals highly degenerate levels, so-called Landau levels. The interesting physics of such a system may also be obtained in rapidly rotating ultracold atoms, due to the physical equivalence of two systems. The system of rapidly rotating Fermi gases in an isotropic harmonic trap has been studied [68], in which the density profiles reveal a step-like structure, similar to the density profiles in quantum Hall effect.

There are different methods in rotating the atomic gases in experiments. The most common method is the pumping of angular momentum to the cloud and later trapping the gas [51, 52]. In this method the isotropic trap is used to preserve the angular momentum. Other possibility is to create a rotating anisotropic trap with a fixed rotation frequency, then the system settles in its ground state at some fixed rotation frequency

[69]. The latter method in rotating ultracold atoms ensure that the anisotropy of the system can also be controlled, which allows the study of the effect of anisotropy on the cloud of atomic gases, specially to make a smooth change of dimension from two dimensional regime for small anisotropies to one dimensional regime when the anisotropy is very large. Later we will show that the single particle wavefunction for a particle in an anisotropic harmonic trap has the interesting property of achieving a smooth transition from a two dimensional regime to a strip-like quasi-one dimensional system. Moreover, the anisotropy of the system in rapidly rotating condensates allows the investigation of properties of interacting Bose gases in one dimensional strip [70, 71, 72]. However the crossover from two dimensions to one dimension would not be so easy, since the existence of interactions in the system complicates the observation of such a transition.

Here we aim to study the effects of anisotropy on density profiles of rapidly rotating ultracold fermionic atoms in a harmonic trap. Since spin polarized fermions are non-interacting because of the Pauli suppression of s-wave scattering, there will be no further parameters appearing in the equation which simplifies the evaluation of the Hamiltonian, considerably. In the next section, a brief review of the results of rapidly rotating fermions in an isotropic harmonic trap [68] is given, reproducing the density profiles and the analytical description of density structure. The effect of temperature on density of rapidly rotating Fermi gases is studied. Then the effect of anisotropy on density profiles of fast rotating ultracold Fermi gases is investigated. A detailed description of the solutions of a particle in a rotating anisotropic trap, already obtained by A. L. Fetter [73] is given. Afterward, the results of our study on the effects of anisotropy on density profiles of the rapidly rotating cold fermions are presented [74]. The chapter ends with the discussions of experimental consequences, and a short conclusion of the study.

2.1 Rapidly rotating Fermions: isotropic case

We start with the single particle physics considering an atom in a two dimensional rotating isotropic trap. We review the solutions for such a system, giving the expressions for energy eigenvalues and corresponding energy eigenfunctions. The Hamilto-

nian describing a particle in the rotating frame is

$$H = \frac{1}{2M}p^2 + \frac{1}{2}M\omega^2 r^2 - \Omega L_z, \quad (2.1)$$

where \mathbf{r} and \mathbf{p} are the two dimensional position and momentum operators in the $x - y$ plane. The system is stable when the rotation frequency is smaller than the confining frequency $\Omega \leq \omega$. The Hamiltonian can be diagonalized applying two successive canonical transformations. First, we apply the usual transformation of the position and momentum operators to the annihilation and creation operators in the Hamiltonian Eq. (2.1), H . The new operators are given by

$$\begin{aligned} a_x &= \sqrt{\frac{M\omega}{2\hbar}} \left(x + \frac{ip_x}{M\omega} \right) \\ a_y &= \sqrt{\frac{M\omega}{2\hbar}} \left(y + \frac{ip_y}{M\omega} \right). \end{aligned} \quad (2.2)$$

a_x^\dagger , and a_y^\dagger can be easily obtained from above equations. Then the new Hamiltonian can be written as

$$H = \hbar\omega \left[a_x^\dagger a_x + a_y^\dagger a_y \right] - \hbar\Omega i \left(a_x a_y^\dagger - a_x^\dagger a_y \right) + \hbar\omega. \quad (2.3)$$

Another transformation to new creation and annihilation operators leads to the diagonalized Hamiltonian

$$\begin{aligned} A &= \frac{1}{\sqrt{2}} (a_x + ia_y) \\ B &= \frac{1}{\sqrt{2}} (a_x - ia_y). \end{aligned} \quad (2.4)$$

The operators A^\dagger , and B^\dagger can be obtained using above equations. Eventually, the diagonalized Hamiltonian is obtained which has the form

$$H = \hbar(\omega + \Omega) A^\dagger A + \hbar(\omega - \Omega) B^\dagger B + \hbar\omega. \quad (2.5)$$

Now one can write the energy eigenvalues as

$$E_{mn} = n\hbar\omega_- + m\hbar\omega_+ + \hbar\omega, \quad (2.6)$$

where $\omega_\pm = (\omega \mp \Omega)$, $n \geq 0$ labels the so called Landau levels, and $m \geq 0$ counts the sublevels in each Landau level. Figure 2.1 describes the graphical correspondence of

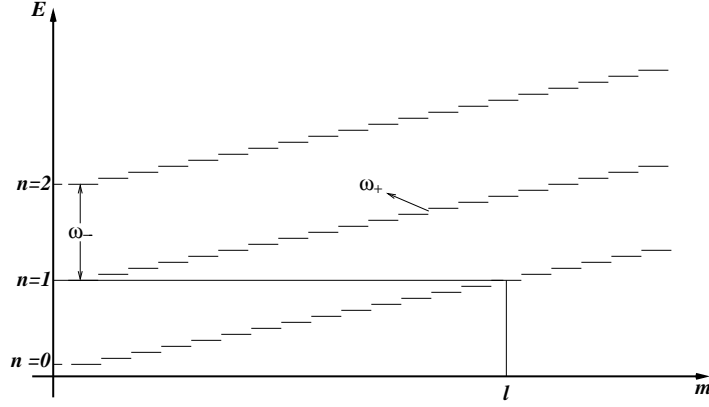


Figure 2.1: Energy vs. number of states in each Landau levels. l is the highest number of states within LL's before the next LL is excited.

the Landau levels and the substates between levels. The corresponding eigenfunctions of the system can be obtained as well which have the form

$$\phi_{nm} = \frac{1}{\sqrt{\pi a^2 n! m!}} e^{r^2/2a^2} \partial_-^n \partial_+^m e^{-r^2/a^2}, \quad (2.7)$$

where $\partial_{\pm} = (\partial_x \pm i\partial_y)$, and $a = \sqrt{\hbar/M\omega}$ is the characteristic harmonic oscillator length.

Since the space wavefunctions are known for the system, the density for non-interacting fermions can be easily obtained by summing over single particle states. Then the density at zero temperature can be written as

$$\rho(x, y) = \sum_{nm} |\phi_{nm}(x, y)|^2 \theta(\mu - E_{nm}), \quad (2.8)$$

where the θ -function counts the number of states below the Fermi level, and μ is the chemical potential determined by the number of particles, N in the system with the constraint

$$N = \int dx dy \rho(x, y). \quad (2.9)$$

The nature of the wavefunctions provides a relatively easy computational calculations, since they are composed of a gaussian multiplied by a Hermite polynomial. The Hermite polynomials, like other orthogonal polynomials satisfy a recursion relation [75]

$$H_{n+1}(x) = 2xH_n(x) - 2nH_{n-1}(x). \quad (2.10)$$

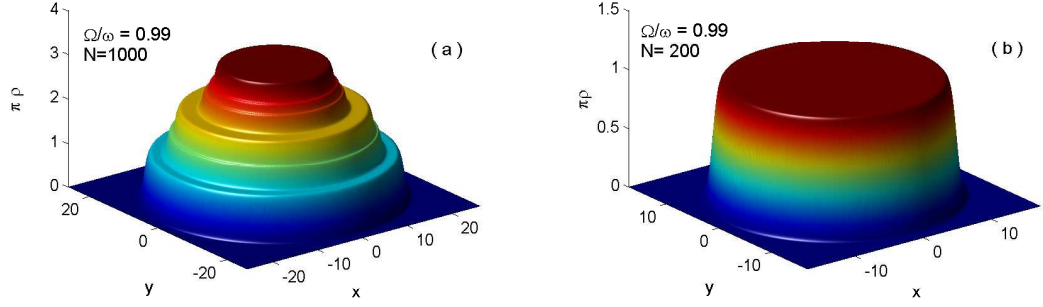


Figure 2.2: (a) Density profile for fermions filling three Landau levels. The Landau levels are represented by a disk like structure. (b) Density profile for fermions occupying the lowest Landau level.

We reproduced the results for the density of fermions in harmonic traps with fast rotation, which were already calculated in detail by Ho [68]. We do the calculations in dimensionless units, using oscillator length $a = \sqrt{\hbar/M\omega}$, frequency ω , and energy quantum $\hbar\omega$, to scale the lengths, frequencies and energies, respectively. Density profiles, in Fig. (2.2) reveals the step structure of fermion density in a rotating trap. Each step in the density profiles is clearly linked with a Landau level, and defines a disc like area of almost constant density. One can obtain the density contribution of each Landau level, but before that let us look at some properties of the density profiles. The first point observed in the density profiles is the existence of the oscillations between two successive steps. The number of oscillations is related to the number of Landau levels. In more explicit words, there are n oscillations in the density when switching between the n^{th} step and $(n+1)^{th}$ steps, a feature which can be clearly seen in the figure. The other point is the maximum number of particles in each Landau plateau, which can be easily determined from the energy eigenvalue expression Eq. (2.6),

$$m_{max} = \text{Int} \left[\frac{\mu/\hbar - n\omega_- - \omega}{\omega_+} \right]. \quad (2.11)$$

The expression obviously shows the step structures of the density, since the maximum number of the particles in lower plateaus is larger than those in upper plateaus. Figure 2.1 explains the phenomenon in more explicit language.

Another feature of density profiles is about the area that each plateau occupies. In

order to calculate it we need to know the radii of the plateaus. Since the system is rotationally symmetric, the function in Eq. (2.7) is also an eigenfunction of L_z , the angular momentum operator, with eigenvalue of $\hbar(m - n)$. The eigenfunction in Eq. (2.7) also satisfies the relationship [36]

$$\hbar \int d^2r \phi^*(r) L_z \phi(r) = \hbar \frac{\langle r^2 \rangle}{a^2} - \hbar. \quad (2.12)$$

Here $\phi(r)$ is the wavefunction for the system. Thus one can simply find the radii for the density of fermions as

$$\langle r^2 \rangle_n = a^2 \left(\frac{\mu - 2(n+1)\hbar\Omega}{M\omega\omega_+} \right). \quad (2.13)$$

The above relation gives us a result about the density profile which shows that the difference between areas of two successive plateaus is always constant. In more detail, it is the difference between the square of radius for two successive plateaus and determined as

$$r_n^2 - r_{n+1}^2 = a^2 \left(\frac{2\Omega}{\omega_+} \right). \quad (2.14)$$

We calculate the density sum of fermions in a more explicit form to obtain a better understanding of the profiles. Here we focus on the lowest Landau Level (LLL), i.e. when $n=0$ to avoid the mathematical difficulties in calculating the whole density sum. Since the density is reduced to sum over the states in LLL we need to obtain the eigenfunctions for this level. The eigenfunctions in LLL are composed of a Gaussian multiplied by a polynomial. Then the density related to this level can be written as

$$\begin{aligned} \rho_{LLL}(r) &= \sum_{m=0}^{m_{max}} |\phi_{0m}(r)|^2 \\ &= \frac{1}{\pi a^2} \sum_{m=0}^{m_{max}} \frac{1}{m!} \left(\frac{r^2}{a^2} \right)^m e^{-\frac{r^2}{a^2}} \\ &= \frac{1}{\pi a^2} \left[1 - e^{-\frac{r^2}{a^2}} \sum_{m=m_{max}}^{\infty} e^{-\ln(m!)} \left(\frac{r^2}{a^2} \right)^m \right] \end{aligned} \quad (2.15)$$

Eventually the sum can be evaluated using the Stirling's approximation [75], and then integrating over m gives the final result for density in LLL as

$$\rho_{LLL} = \frac{1}{2\pi a^2} \left[1 + \operatorname{erf} \left(\frac{r^2/a^2 - m_{max}}{\sqrt{2r/a}} \right) \right] \quad (2.16)$$

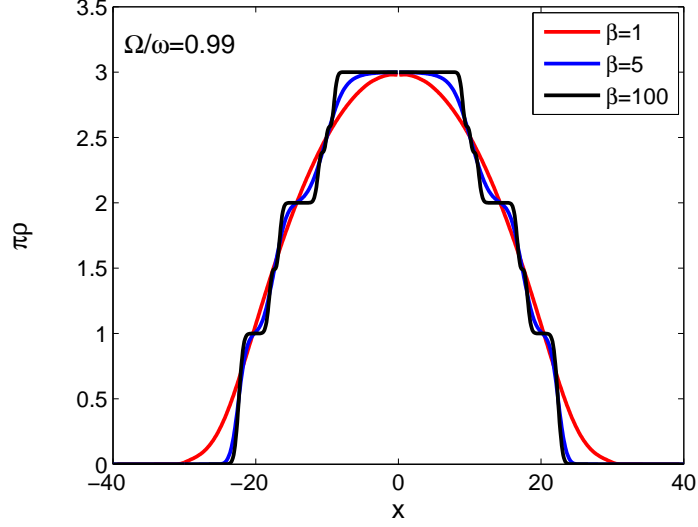


Figure 2.3: Density profile for fermions at different temperatures and at $\Omega/\omega = 0.99$. The layered aspect of the profile is eliminated by temperature.

Note that the error function, $\text{erf}(x)$, appearing in equation above ensures that the contribution of LLL to the density is constant. Ho claims that the densities for higher Landau levels can be obtained from the LLL density expression and shows that their contribution to the density is also constant [68]. The density profiles given in the previous calculations are all calculated at zero temperature. The effects of temperature on density profiles can be calculated by including the Fermi distribution function as

$$\rho(x, y) = \sum_{nm} |\phi_{nm}(x, y)|^2 \frac{1}{\exp[\beta(E_{nm} - \mu)] + 1}, \quad (2.17)$$

where $\beta = 1/k_B T$ is the inverse temperature.

We calculated density profiles at finite temperatures by choosing appropriate values for inverse temperature. The step structure of the density profile is smeared out when the temperature is high enough $k_B T \sim \hbar\omega_-$, such that thermally excited particles can occupy a higher Landau level, as can be seen in Fig. (2.3). The calculated density profiles show that the step structure becomes indiscernible, as the transition regions between the Landau level steps dominate the profile. For larger temperatures the profile assumes the gaussian profile as would be expected from a Boltzmann gas.

The results for rapidly rotating fermions in an isotropic harmonic trap will help us to understand the properties of rapidly rotating fermions in an anisotropic harmonic trap

which is discussed in the next section.

2.2 Rapidly rotating fermions: anisotropic case

In this section, we consider a system of ultracold Fermi gas in a rotating anisotropic trap. Density profiles for different control parameters of the system are calculated. The discussions throughout the section will be limited to behavior in two dimensions. However, before discussing the results for density profiles we will focus on the physics of switching between one and two dimensional regimes. To extend the results to the third dimension two limits must be noted; the strong confinement, or a slowly varying potential along the third dimension [68]. With these conditions satisfied, which are also realized in experiments of ultracold atoms the extension to three dimension could be carried out.

To study the effect of anisotropy on the density of the fermions, it is instructive to understand the physics of a single particle in a two dimensional rotating anisotropic trap. We first start with the Hamiltonian describing such a system which can be written as

$$H = \frac{1}{2M} (p_x^2 + p_y^2) + \frac{1}{2} M \omega_x^2 x^2 + \frac{1}{2} M \omega_y^2 y^2 - \Omega L_z. \quad (2.18)$$

in the rotating frame. Here M is the mass of the particle, the angular momentum in the z direction is given as $L_z = x p_y - y p_x$, and Ω is the rotation frequency. The trapping frequencies along the x and y directions are ω_x , and ω_y , respectively. Without loss of generality we take $\omega_y \geq \omega_x$, and refer to the y and x directions as the strongly confined and weakly confined directions. Since the stability of trapped systems depends on the rotation frequency, the condition for stability enforce a smaller rotation frequency with respect to the weak confining frequency $\Omega \leq \omega_x$. The eigenenergies of the system can be obtained by direct diagonalization of Hamiltonian [76] or applying two successive Bogoliubov transformations [77]

$$E_{n,m} = n \hbar \omega_- + m \hbar \omega_+ + \frac{1}{2} \hbar (\omega_- + \omega_+), \quad (2.19)$$

where n and m are positive integers. Two different frequency modes in the energy

expression are defined to be

$$\omega_{\pm}^2 = \frac{1}{2}(\omega_x^2 + \omega_y^2) + \Omega^2 \mp \sqrt{\frac{1}{4}(\omega_y^2 - \omega_x^2)^2 + 2(\omega_x^2 + \omega_y^2)\Omega^2}. \quad (2.20)$$

In the isotropic limit, energy eigenvalues are obtained by substituting $\omega_y = \omega_x = \omega$, which results in the simple expression for $\omega_- = \omega + \Omega$, and $\omega_+ = \omega - \Omega$ introduced in the previous section. The frequency modes represent two different motions of the particle in the trap, which have the form

$$\begin{aligned} x_+(t) &= x_0 e^{-i\omega_+ t} & y_+(t) &= i\beta_+ x_0 e^{-i\omega_+ t} \\ x_-(t) &= i\beta_- y_0 e^{-i\omega_- t} & y_-(t) &= y_0 e^{-i\omega_- t} \end{aligned} \quad (2.21)$$

where the anisotropy of single particle orbits are controlled by two dimensionless parameters

$$\begin{aligned} \beta_+ &= \frac{\omega_x^2 - \omega_+^2 - \Omega^2}{2\Omega\omega_+}, \\ \beta_- &= \frac{\omega_-^2 - \omega_y^2 + \Omega^2}{2\Omega\omega_-}, \end{aligned} \quad (2.22)$$

both of which vary in the $[0,1]$ interval. For the symmetric case $\beta_+ = \beta_- = 1$ reduces the equations above to the known motions of a particle in a circular orbit with positive and negative helicities for plus and minus modes, respectively. The parameters β_+ , and β_- are determined by a detailed analysis of equations of motion for both plus and minus modes.

Although the Hamiltonian in Eq. (2.18) seems to be simple, the real-space functions describing the system were introduced almost recently. Oktel [77] solved the problem in the limit of fast rotation, and very small anisotropy and obtained the wavefunctions for the system, but the general wavefunctions was later obtained by Fetter [73]. We here review the solution in [73] in a relatively detailed fashion (to avoid any confusion and increasing the number of parameters we prefer to follow the notation used by Fetter in discussed paper). Since the diagonalization of the system by introducing usual creation and annihilation operators in quantum mechanics for this system cost considerable algebraic complexity, a canonical transformation is used to solve the problem. The canonical transformation expresses the Hamiltonian in terms of new coordinates and momenta which satisfy the same Poisson brackets or commutation relations. Valatin [78] introduces a useful canonical transformation which gives

a sum of two independent harmonic oscillators from originally rotating single particle Hamiltonian in an anisotropic harmonic trap. The canonical transformation is generated from a generating function involving the old and new coordinates given by

$$S(x, y; Q_+, Q_-) = -M\gamma \left[\lambda_+ \lambda_- Q_+ Q_- + \frac{1}{2}(\lambda_+^2 + \lambda_-^2)xy - \lambda_+ Q_+ y - \lambda_- Q_- x \right]. \quad (2.23)$$

Here λ_{\pm} are dimensionless parameters defined as

$$\lambda_{\pm} = \frac{\omega_{\pm}}{\omega_{\pm} + \beta_+ \beta_- \omega_{\mp}}, \quad (2.24)$$

and γ is a frequency with the definition

$$\gamma = \frac{\omega_-^2 - \omega_+^2}{2\Omega}. \quad (2.25)$$

The canonical momenta corresponding to coordinates are obtained from generating function derivatives [79] as follows

$$\begin{aligned} p_x &= \frac{\partial S}{\partial x} & p_y &= \frac{\partial S}{\partial y} \\ P_+ &= -\frac{\partial S}{\partial Q_+} & P_- &= -\frac{\partial S}{\partial Q_-}. \end{aligned} \quad (2.26)$$

A more detailed calculation give the relations between original coordinates and new canonical variables as

$$\begin{aligned} x &= \lambda_+ Q_+ - \frac{P_-}{M\gamma\lambda_-}, \\ y &= \lambda_- Q_- - \frac{P_+}{M\gamma\lambda_+}. \end{aligned} \quad (2.27)$$

Now, by substituting the relations above into the Eq. (2.18), the Hamiltonian can be diagonalized and rewritten in the form

$$H = \frac{P_+^2}{2M} + \frac{1}{2}M\omega_+^2 Q_+^2 + \frac{P_-^2}{2M} + \frac{1}{2}M\omega_-^2 Q_-^2. \quad (2.28)$$

The new Hamiltonian is a sum of two separated harmonic oscillators which is already diagonalized. By defining the well known creation and annihilation operators for two parts as

$$\begin{aligned} \alpha_{\pm} &= \frac{1}{\sqrt{2}} \left(\frac{Q_{\pm}}{d_{\pm}} + i \frac{d_{\pm} P_{\pm}}{\hbar} \right) \\ \alpha_{\pm}^{\dagger} &= \frac{1}{\sqrt{2}} \left(\frac{Q_{\pm}}{d_{\pm}} - i \frac{d_{\pm} P_{\pm}}{\hbar} \right) \end{aligned} \quad (2.29)$$

one can write the Hamiltonian in terms of these operators. Here $d_{\pm} = \sqrt{\hbar/M\omega_{\pm}}$. Now we can write the ground state eigenfunction for the system in a straight forward manner as we know from quantum mechanics

$$\phi_{00}(Q_+, Q_-) \propto \exp\left(-\frac{Q_+^2}{2d_+^2} - \frac{Q_-^2}{2d_-^2}\right). \quad (2.30)$$

The higher excited states are obtained by applying the creation operators on the ground state wavefunction. Note that the eigenfunctions are in terms of new coordinates and must be transformed to the original coordinates. Valatin uses the generating function $S(x, y; Q_+, Q_-)$ to carry out the transformation [78]. Let us here write the transformation itself and leave the proof to be done in Appendix A. The relation

$$\phi_{00}(x, y) \propto \int \int dQ_+ dQ_- e^{\frac{i}{\hbar} S(x, y, Q_+, Q_-)} \phi_{00}(Q_+, Q_-) \quad (2.31)$$

gives the ground state wavefunction in original coordinates. Finally, evaluating the integral gives the expression for the ground state as

$$\phi_{00} = \frac{1}{\sqrt{\pi a_x a_y}} \exp\left[-\frac{x^2}{2a_x^2} - \frac{y^2}{2a_y^2}\right] \exp\left\{i \frac{Mxy}{\hbar} \left[\frac{\gamma}{1 + \beta_+ \beta_-} - \frac{1}{2} \left(\frac{\omega_+}{\beta_+} + \frac{\omega_-}{\beta_-}\right)\right]\right\}, \quad (2.32)$$

where a_x and a_y are the widths of the Gaussian envelope

$$a_x^2 = \frac{1 + \beta_+ \beta_-}{\beta_+} \frac{\hbar}{M\gamma}, \quad a_y^2 = \frac{1 + \beta_+ \beta_-}{\beta_-} \frac{\hbar}{M\gamma}. \quad (2.33)$$

The wavefunctions in the lowest Landau level (LLL) are found by applying the relevant raising operator which are given by

$$\phi_{m0}(x, y) = \frac{1}{\sqrt{m!}} \left(\frac{c}{2}\right)^{m/2} H_m\left(\frac{\xi_+}{\sqrt{2c}}\right) \phi_{00}(x, y), \quad (2.34)$$

where H_m is the m^{th} Hermite polynomial. Here

$$c = \frac{1 - \beta_+ \beta_-}{1 + \beta_+ \beta_-}. \quad (2.35)$$

which controls the switching between the one and two dimensional regimes as we show in the following sections.

The relevant raising operators are applied to the ground state wavefunction, to obtain the wavefunctions in lowest and higher Landau levels. We suggest a general form for the wavefunctions in higher Landau levels as

$$\begin{aligned} \phi_{nm}(x, y) &= \frac{1}{\sqrt{n!m!}} \phi_{00}(x, y) \\ &\times \sum_{k=0}^n \left[(-i)^{n-k} \frac{2^{n-k}}{(n-k)!} \rho^{n-k} \frac{d^{n-k}}{d^{n-k} \xi_-} P_n(\xi_-) \frac{d^{n-k}}{d^{n-k} \xi_+} P_m(\xi_+) \right], \end{aligned} \quad (2.36)$$

where

$$P_m(\xi_{\pm}) = \left(\frac{c}{2}\right)^{n/2} H_m\left(\frac{\xi_{\pm}}{\sqrt{2c}}\right), \quad (2.37)$$

ξ_{\pm} are two complex coordinates which control motion in Landau levels

$$\begin{aligned} \xi_+ &= \sqrt{\frac{2M\gamma\beta_+}{\hbar}} \frac{x + i\beta_-y}{1 + \beta_+\beta_-}, \\ \xi_- &= \sqrt{\frac{2M\gamma\beta_-}{\hbar}} \frac{y + i\beta_+x}{1 + \beta_+\beta_-}, \end{aligned} \quad (2.38)$$

and $\rho = \sqrt{\beta_+\beta_-/(1 + \beta_+\beta_-)}$.

It is obviously seen from Hamiltonian Eq. (2.18), that the system is described by two dimensionless parameters, the anisotropy

$$\tilde{\omega}_y = \frac{\omega_y}{\omega_x} \geq 1, \quad (2.39)$$

and the scaled rotation frequency

$$\tilde{\Omega} = \frac{\Omega}{\omega_x} \leq 1. \quad (2.40)$$

Other quantities can be scaled and non-dimensionalized applying appropriate scalings. In particular, we scaled the lengths by the oscillator length in the x direction $l_x = \sqrt{\hbar/M\omega_x}$, frequencies by ω_x and energies by $\hbar\omega_x$. The calculations in this section are also done in dimensionless units.

The wavefunctions introduced above exhibit a remarkable structure. The anisotropic cloud in the case of rapid rotation becomes almost one dimensional strip [70, 71]. The wavefunction also continuously connects the Hermite polynomials appearing in wavefunctions of the two dimensional rotating anisotropic system to the usual one dimensional oscillator wavefunctions. To be more explicit, in the case of isotropic limit an m^{th} order zero settles at the origin for the m^{th} wavefunction. With the anisotropy turned on, the m^{th} order zero immediately breaks up into m first order zeros along the weak anisotropy direction [77]. As seen in Fig. (2.4), by increasing the anisotropy of the system the roots of the Hermite polynomial, which is an analytical function in LLL, are separated. Such a separation of roots causes more anisotropy in density profile. We discuss the transition between the two and one dimensional regimes in more details in the next section, by introducing a parameter which corresponds to the maximum number of states between two successive Landau levels.

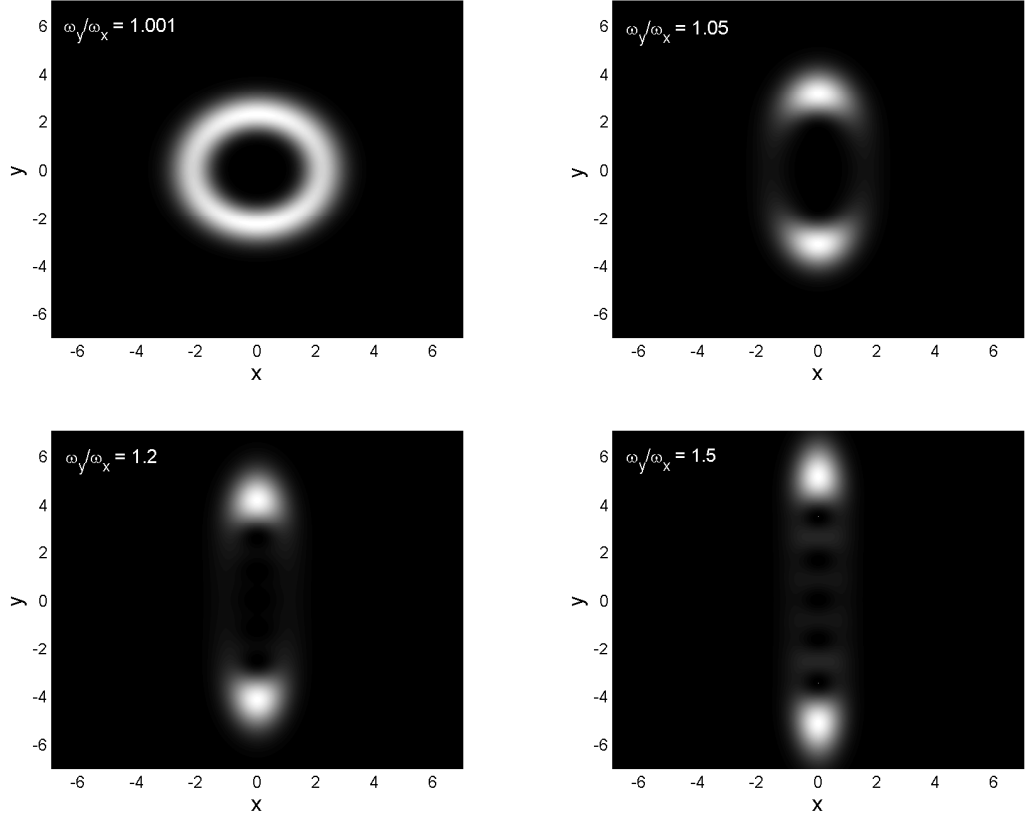


Figure 2.4: Density of fifth wavefunction at different anisotropies, and fixed rotation frequency, $\Omega/\omega_x = 0.99$. Increasing the anisotropy breaks up the fifth order zeros in the origin to row of zeros along the weak trapping direction.

2.2.1 One and two dimensional regimes

The number of states in a Landau level that have the energy value lower than the energy of any state in the higher Landau level is a good identifier to discuss the transition from two to one dimensional regimes. The physical significance of this quantity is embedded in the energy spectrum of the system given in Eq. 2.19. It would be quite instructive to look at the energy spectrum of two limiting cases. One is the case for a system of rotating isotropic trap expressed by

$$E_{nm} = \hbar \left[\left(n + \frac{1}{2} \right) (\omega + \Omega) + \left(m + \frac{1}{2} \right) (\omega - \Omega) \right], \quad (2.41)$$

and the other one is the case for non-rotating anisotropic trap given by

$$E_{n_x n_y} = \hbar \left[\left(n_x + \frac{1}{2} \right) \omega_x + \left(n_y + \frac{1}{2} \right) \omega_y \right]. \quad (2.42)$$

The spectra reveal an interesting fact, both have the same structures since they have been expressed in terms of two non-negative integers. The structure can be graphically represented by figure 2.1. The number of the states between two levels is tightly connected to the dimensionality of the systems. The rotating anisotropic trap system interpolates between these two limits, and we expect that such number could be a good identifier for this interpolation. Thus, we define

$$l = \frac{\omega_-}{\omega_+}, \quad (2.43)$$

Let us study l in more detail, by demonstrating its behavior in terms of anisotropy, an important parameter in changing the geometry of the system. Figure 2.5 explicitly shows the sort of changes in l as a function of anisotropy, ω_y at a fixed rotation frequency, Ω . It is clearly seen that l has a minimum value at a certain anisotropy. It starts from its isotropic value

$$l_{iso} = \frac{1 + \tilde{\Omega}}{1 - \tilde{\Omega}} \quad (2.44)$$

for $\tilde{\omega}_y = \tilde{\omega}_x = 1$, and decreases sharply as

$$l = l_{iso} \sqrt{\frac{(1 - \tilde{\Omega})(\tilde{\omega}_y + \tilde{\Omega})}{(1 + \tilde{\Omega})(\tilde{\omega}_y - \tilde{\Omega})}} \quad (2.45)$$

to reach its minimum of $l_{\min} = \sqrt{8/(1 - \tilde{\Omega}^2)}$, which occurs at the critical anisotropy value

$$\tilde{\omega}_y = \sqrt{1 + 4\tilde{\Omega}^2}. \quad (2.46)$$

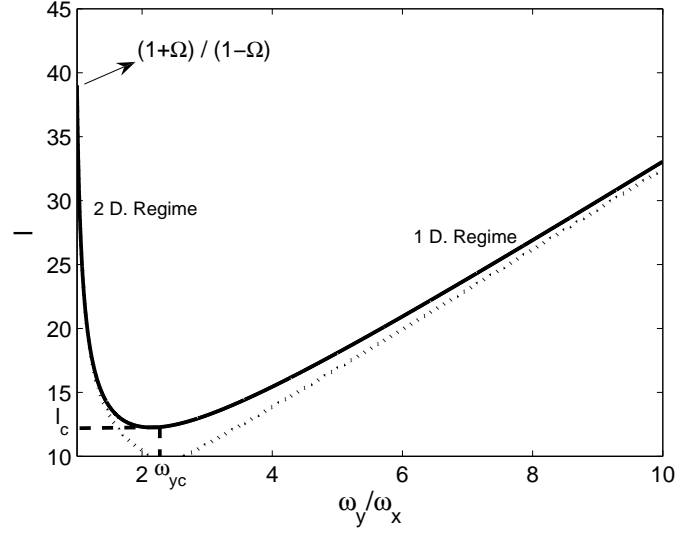


Figure 2.5: Solid line shows the behavior of l , maximum number of states within two LL's as a function of the anisotropy of the system ω_y/ω_x . Dashed lines are the asymptotic results for one and two dimensional limits. Here $\omega_{yc} = (1 + 4\Omega^2/\omega_x^2)^{1/2}$ is the critical anisotropy where l is minimum. The minimum number of states is given by $l_c = (\frac{8}{1-\Omega/\omega_x})^{1/2}$

After this point the increase in anisotropy causes an enlargement in the number of states between two successive Landau levels

$$l = \sqrt{\frac{\tilde{\omega}_y^2 + 3\tilde{\Omega}^2}{1 - \tilde{\Omega}^2}} \simeq \frac{\tilde{\omega}_y}{\sqrt{1 - \tilde{\Omega}^2}}, \quad (2.47)$$

which is linear in ω_y for large anisotropies.

An important point here is the high degeneracy of the Landau levels in the case of the isotropic systems. Such a high degeneracy for an anisotropic systems is only obtained for large asymmetries in trap frequencies. This large degeneracy for the case of two dimensional regimes is caused by the Coriolis force canceling the trapping force. This mechanism freezes the kinetic energy of the particles partially, and for a larger rotation frequency the degeneracy will also increase. However, the case for the large anisotropy is completely different. In this regime the energy spectrum is like a subband quantization in a narrow channel where the states in each Landau level have the same wavefunction along the tightly confined direction.

The form of the wavefunctions also support this identification based on l . For low

anisotropy the wavefunctions peak around an ellipse in the $x - y$ plane, while in the one dimensional regime the density in the x direction shows prominent oscillations, similar to one dimensional harmonic oscillator wavefunctions. Based on the discussions here it is expected that the density of the fermionic system exhibits different forms in these two regimes, the fact that we show in the next section.

2.2.2 Density Profiles

The procedure for calculating the density profiles is the same as was illustrated in isotropic case. Here we consider N fermionic atoms which are non-interacting with the wavefunction known from the previous section. Our task is only to sum over filled single particle states controlled by the chemical potential. The density is calculated using Eq. (2.8). The numerical calculations can be done with a very low computational cost, with high accuracy since the wavefunctions composed of a gaussian multiplied by Hermite polynomials, benefit the recursive structure also discussed in previous sections. This enables us to calculate the density profiles up to thousands of particles rapidly. The parameters can be controlled to obtain the profiles with particles in the lowest six Landau levels, which are given in Appendix B.

The density profiles are calculated for different values of anisotropy for $N = 1000$ at fixed rotation frequency $\Omega/\omega_x = 0.999$, all displayed in figure 2.6. We specially calculated the density for very small anisotropy, critical value of anisotropy (where l reaches its minimum value), and for high anisotropy. The profiles show a step structure for small anisotropy, the same as what we see for the isotropic density profiles, but here, the disk-like plateaus are now elliptical. However, the step structure is only observed in Fig. (2.6a). Each plateau corresponds to a Landau level, which are separated with a small region of switching. We show that these plateaus have almost constant density proportional to $\frac{M\gamma}{2\pi\hbar}$. Since the numerical calculations are given in dimensionless units, each step in a profile has a density of an integer times $\frac{\gamma}{2\pi\omega_x}$.

The oscillations in switching between two successive steps exist here but in a more noticeable form. For small anisotropy values the same behavior is observed, i.e. there are n oscillations in the density when switching between the n^{th} step and $(n + 1)^{th}$ steps. However, for higher values of anisotropy oscillations in density along the weak

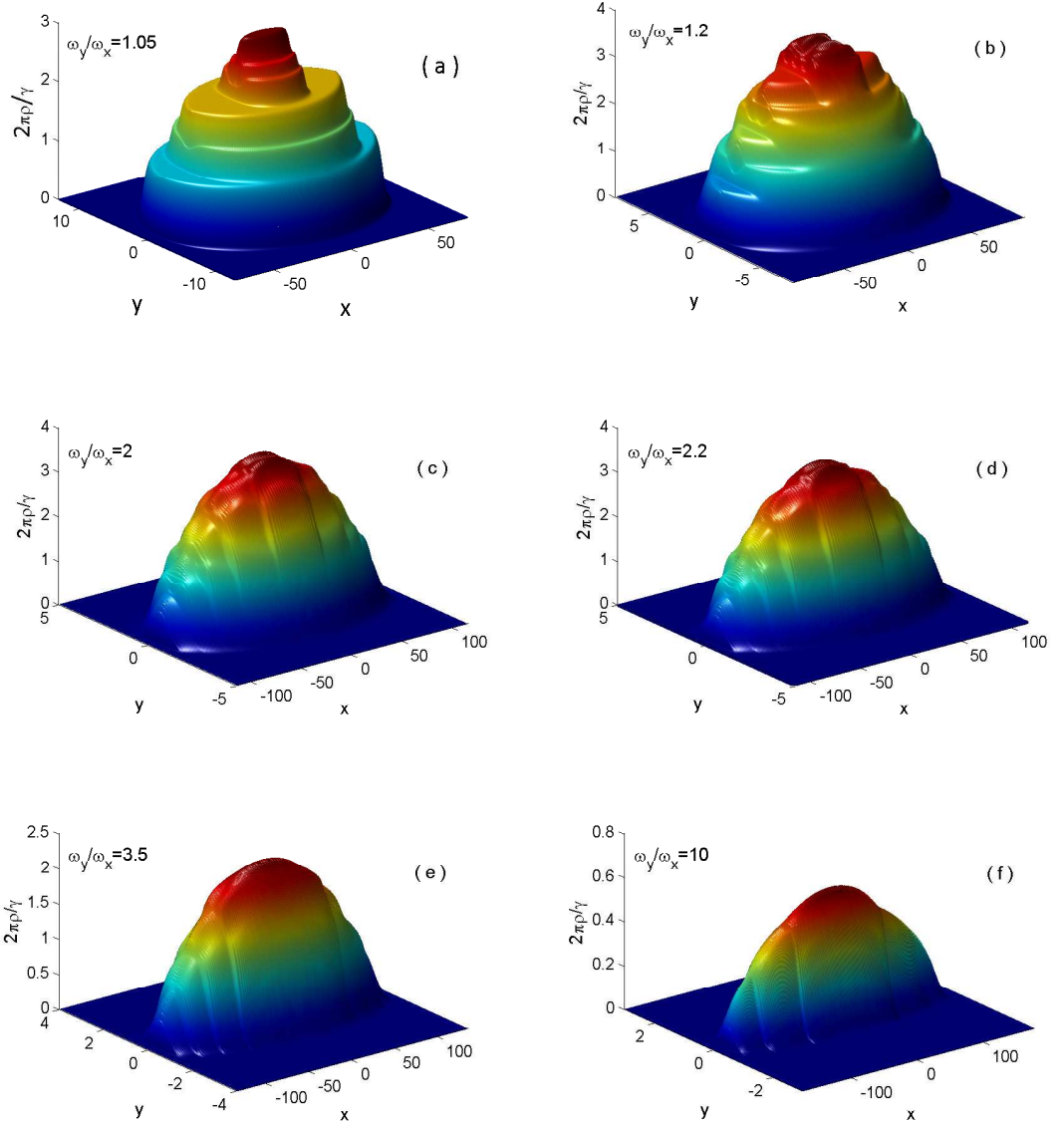


Figure 2.6: Density profiles for fermions at different anisotropy values of the system and fixed number of the particles $N=1000$, and fixed rotation frequency $\Omega/\omega_x = 0.999$. The Friedel oscillations are observed in density profiles of anisotropic cases. The number of LL's that fermions fill at each anisotropy can also be determined by counting the number of plateaus in the density profiles.

confinement direction become more prominent. The anisotropy also changes the step structure of the density profiles, smearing out the level structures. The change starts around the critical anisotropy value, ω_{yc} as seen from Fig. (2.6c) The transition between Landau levels do not take place with clear steps, but the oscillations become dominant in profiles. These oscillations are related to sharp cutoffs in Fermi surface in momentum space. In solid state physics, they are known as Friedel oscillations [80].

A drastic change happens in density profiles when the anisotropy is very large. In this limit, the density profiles exhibit new shape of being a gaussian along the strong trapping direction and a semicircular shape along weak trapping direction. The shape of density in weak direction is what we know from trapped fermions in one dimension. In the step structure one can easily count the number of Landau levels filled, and here now can determine Landau levels with the semicircular shape of each level in the density profile. This fact is obviously seen in Fig. (2.6e).

The change in the shape of density profiles when switching from two dimensional to one dimensional regime can be seen for a profile with only one level filled, which naturally is the LLL. We choose a small number of particles with respect to the previous calculations to ensure that the particles settle only in LLL for any anisotropy of the system. As seen in Fig. (2.7), the plateau form of density for the LLL changes to be semicircular. The Friedel oscillations are also observed to be more prominent when the anisotropy is increased. Again, the changes in the shape of the density and also in the oscillations starts around the critical anisotropy value.

The analytical investigation of density sum Eq. (2.8) may help us to understand the different aspects of profiles in more detail. To avoid the algebraic complexities we focus on the case that all the atoms settle in the LLL. Then, we write the density sum for N fermions which is explicitly

$$\begin{aligned}\rho(x, y) &= \sum_{m=0}^N |\phi_{0m}(x, y)|^2 \\ &= \frac{1}{\pi a_x a_y} e^{-x^2/a_x^2 - y^2/a_y^2} \sum_{m=0}^N \frac{1}{m!} \left(\frac{c}{2}\right)^m H_m\left(\frac{\tilde{\xi}_+}{\sqrt{2c}}\right) H_m\left(\frac{\xi_+}{\sqrt{2c}}\right).\end{aligned}\tag{2.48}$$

We concentrate in the limit $N \rightarrow \infty$, which enables us to evaluate the sum using

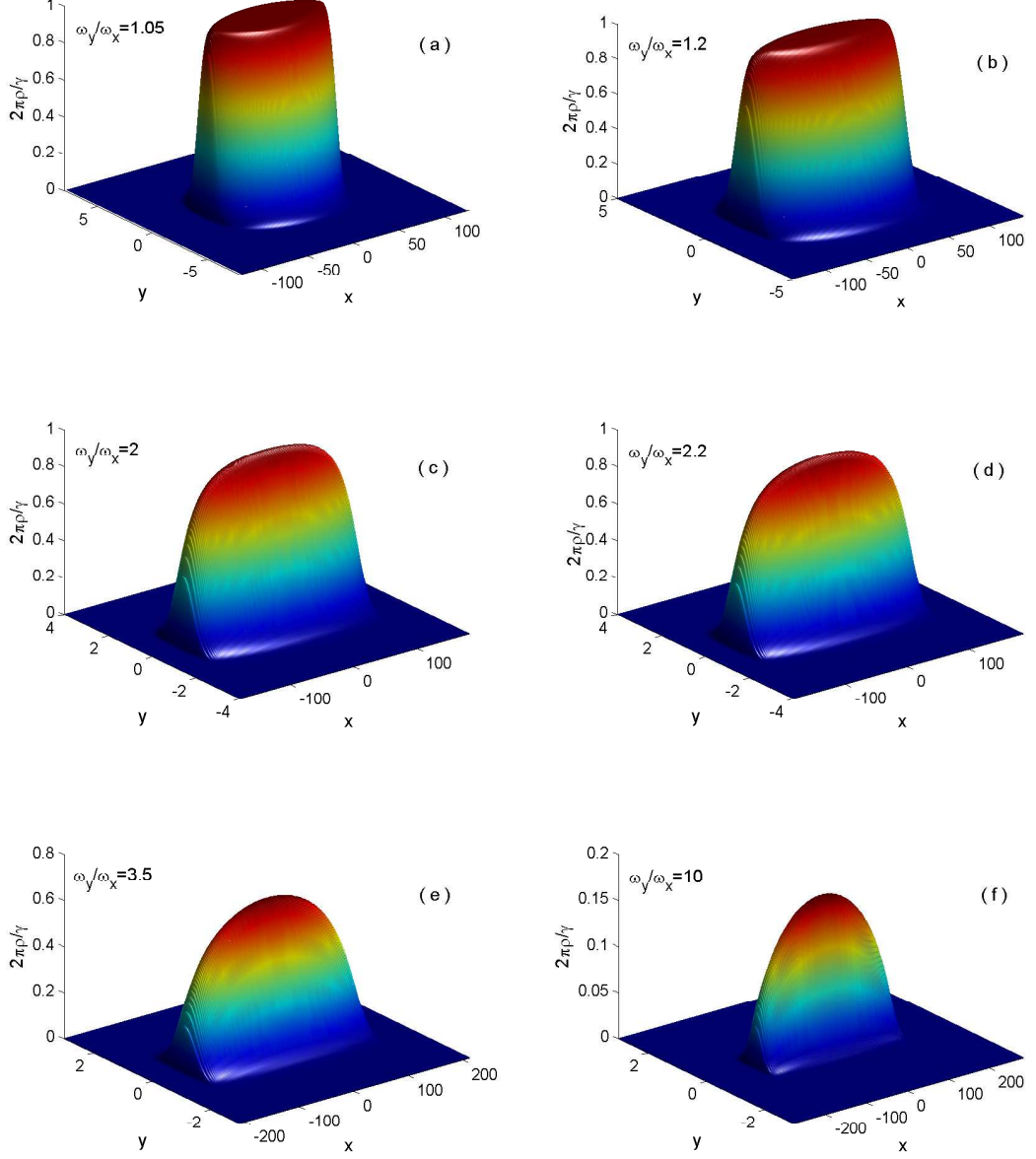


Figure 2.7: Density profiles of fermions at different anisotropy values of the system and fixed number of the particles $N=200$, and fixed rotation parameter $\Omega/\omega_x = 0.9999$, when all the fermions are settled at the LLL. The Friedel oscillations are also observed for density profiles of anisotropic cases.

the generating function for Hermite polynomials. We now rewrite the sum in a more compact form defining $z = \xi_+ / \sqrt{2c}$, then we have

$$S(\bar{z}, z) = \sum_{m=0}^{\infty} \frac{1}{m!} \left(\frac{c}{2}\right)^m H_m(\bar{z}) H_m(z). \quad (2.49)$$

Since the sum is composed of two Hermite polynomials, in which one is the complex conjugate of the other, we use the generating function for Hermite polynomials regarding $t = |t|e^{i\theta}$ to be a complex variable

$$e^{-\frac{c}{2}\bar{t}^2 + \sqrt{2c}\bar{t}\bar{z}} e^{-\frac{c}{2}t^2 + \sqrt{2c}tz} = \sum_m \frac{H_m(z)}{m!} t^m \left(\frac{c}{2}\right)^{m/2} \sum_n \frac{H_n(\bar{z})}{n!} \bar{t}^n \left(\frac{c}{2}\right)^{n/2}, \quad (2.50)$$

An integration helps us to eliminate the extra terms and also one of the sums to obtain the same infinite sum introduced in density expression. Then the right hand side could be written as

$$\sum_{m,n} \frac{1}{m!n!} H_m(z) H_n(\bar{z}) \left(\frac{c}{2}\right)^{\frac{m+n}{2}} \int_0^\infty d|t| 2|t| e^{-|t|^2} |t|^{m+n} \int_0^{2\pi} \frac{d\theta}{2\pi} e^{i(m-n)\theta}, \quad (2.51)$$

which is exactly the infinite sum we need. Then we just need to evaluate the integral in the left hand side

$$S(\bar{z}, z) = \int_0^{2\pi} \frac{d\theta}{2\pi} \int_0^\infty d|t| 2|t| \exp\left[-\frac{c}{2}(\bar{t}^2 + t^2) + \sqrt{2c}(\bar{t}\bar{z} + tz) - |t|^2\right]. \quad (2.52)$$

One may do a change of variables in order to evaluate the resulting Gaussian integral. Defining new variables a , and b through $t = a + ib$ and integrating over a , and b

$$S(\bar{z}, z) = \frac{1}{\sqrt{(1-c)(1+c)}} \exp\left[\frac{1}{2} \frac{c}{1-c} (i(z - \bar{z}))^2\right] \exp\left[\frac{1}{2} \frac{c}{1+c} (z + \bar{z})^2\right], \quad (2.53)$$

and by replacing the $z = \xi_+ / \sqrt{2c}$ and using relation Eq. (2.38) for ξ_+ the sum can be evaluated which gives a constant density

$$\rho(x, y) = \rho_0 = \frac{1}{\sqrt{1-c^2}} \frac{1}{\pi a_x a_y} = \frac{M\gamma}{2\pi\hbar}. \quad (2.54)$$

Through the numerical calculations we observe that the density of the Landau levels is an integer times this constant value. The parameter γ controls the density of plateaus which goes to its isotropic value up to the first order approximation in evaluating the *erf* function appeared in Eq. (2.16) around the center of the cloud. Note that the isotropic value for γ is obtained from Eq. (2.25) which is $\gamma = 2\omega$. For small anisotropies the density reaches the value above quickly, even for small number of

particles since the contribution to the density around the center from higher wave-functions is very small. In the case of large anisotropy, the cloud goes through two very different paths to reach the constant density, with prominent oscillations. As we discussed above the presence of these oscillations are related to a sharp cutoff in the Fermi surface of fermions in momentum space, but they are suppressed in two dimensional regime as locally the maximum allowed density within a Landau level is reached. The frequency of the Friedel oscillations can be obtained with a simple scaling argument. We define two finite sums of Hermite polynomials which are only different in the c parameter,

$$S_N(a, b, c_i) = \sum_{n=0}^N \frac{H_n(\bar{z})H_n(z)}{2^n n!} c_i^n, \quad (2.55)$$

where $i = 1, 2$, and $z = a + ib$. From the infinite sum Eq. (2.53) we can assume that two finite sums to be related

$$S_N(a, b, c_2) \cong \sqrt{\frac{1 - c_1^2}{1 - c_2^2}} S_N\left(\sqrt{\frac{(1 + c_1)c_2}{(1 + c_2)c_1}} a, \sqrt{\frac{(1 - c_1)c_2}{(1 - c_2)c_1}} b, c_1\right), \quad (2.56)$$

for sufficiently large number of particles, i.e. $N \gg 1$. It allows us to choose c_1 arbitrarily close to one,

$$\begin{aligned} S_N(a, b, c_1) &= \sum_{n=0}^N \frac{H_n(\bar{z})H_n(z)}{2^n n!} c_1^n \\ &\approx \sum_{n=0}^N \frac{H_n(\bar{z})H_n(z)}{2^n n!} \\ &= S_N(a, b, 1), \end{aligned} \quad (2.57)$$

provided that $(1 - c_1)N \ll 1$, or for a rapidly rotating trap. Here we have a sum over two orthogonal functions, and using the Christoffel-Darboux formula [81] the sum may be calculated exactly,

$$\begin{aligned} S_N(a, b, 1) &= \sum_{n=0}^N \frac{H_n(\bar{z})H_n(z)}{2^n n!} \\ &= \frac{H_{N+1}(\bar{z})H_N(z) - H_{N+1}(z)H_N(\bar{z})}{2^{N+1} N! (\bar{z} - z)}. \end{aligned} \quad (2.58)$$

The exact evaluation along with a scaling assumption leads us to a relationship for the wavevector of the Friedel oscillations near the center of the trap

$$\rho(x, y = 0) = \rho_0 \left(1 + (-1)^N \frac{1}{4N} \cos(k_F x) \right), \quad (2.59)$$

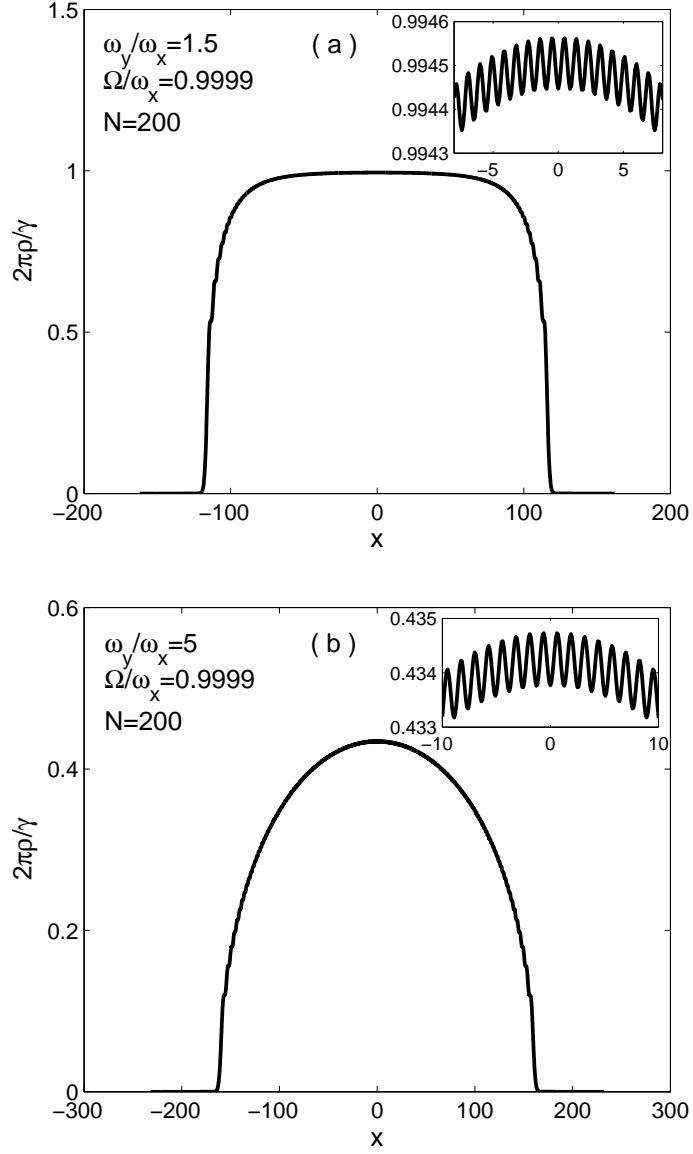


Figure 2.8: (a) Density for $N=200$ fermions at $\Omega/\omega_x = 0.9999$, and $\omega_y/\omega_x = 1.5$. (b) Density for $N=200$ fermions at $\Omega/\omega_x = 0.9999$, and $\omega_y/\omega_x = 5$. The insets in both figures highlight the Friedel oscillation in density profiles of the fermions.

with

$$k_F l_x = \sqrt{8N/\omega_x} \sqrt{\omega_+ + \omega_- \beta_+ \beta_-}. \quad (2.60)$$

The local density approximation (LDA) is a useful tool to investigate the density properties of the system when we have a smooth external potential. In the case of isotropic trap one can describe the system with the Hamiltonian Eq. (1.20). The first term in the Hamiltonian corresponds to a density with a step structure, each step with a constant contribution of $M\Omega/\pi\hbar$. For a rapidly rotating gas the second term, an effective potential, could be supposed to be a slowly varying potential and can be absorbed inside the chemical potential [68]. However, in the case of anisotropic trap, to treat the different behavior of the system we need two different version of LDA, one dimensional LDA (1DLDA), and two dimensional LDA (2DLDA).

The two dimensional regime is the same as the isotropic case, since the effective potential in either strong and weak trapping directions are varying slowly over the range of magnetic length defined by rotation. Such conditions provide us the possibility of treating the system locally homogenous. As we described above each Landau level contribute to the density with a constant value, then the local density in each point will be given by

$$\rho(x, y) = k \frac{M\Omega}{\pi\hbar}, \quad (2.61)$$

where k itself is defined as

$$\begin{aligned} k &= \sum \Theta \left[\mu - M/2(\omega^2 - \Omega^2)r^2 - (2n + 1)\hbar\Omega \right] \\ &= \text{Int} \left[\frac{\mu - M/2(\omega^2 - \Omega^2)r^2 + \hbar\Omega}{2\hbar\Omega} \right]. \end{aligned} \quad (2.62)$$

One may need the useful identity

$$\sum_n \Theta [\alpha(x - n)] = \text{Int}[x + 1], \quad (2.63)$$

to evaluate the sum, where x , and α are positive definite. The numerical calculations for 2DLDA are illustrated in figure 2.9a.

By increasing the anisotropy, the system undergoes a transition from two dimensional regime to an almost one dimensional regime, losing the step structure in density profiles. In this regime the system can not be described by 2DLDA in a correct manner

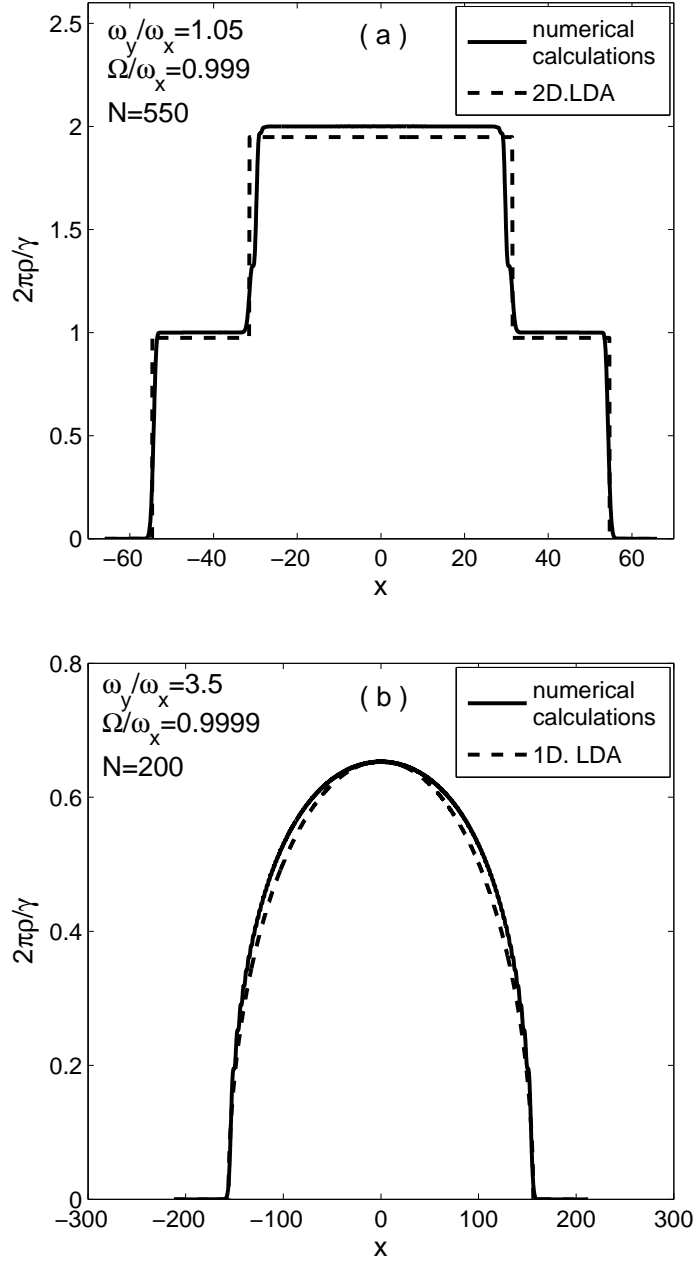


Figure 2.9: (a) Density of $N=550$ fermions obtained by direct numerical calculations (solid line), and two dimensional LDA (dashed line) at $\Omega/\omega_x = 0.999$, and $\omega_y/\omega_x = 1.05$. (b) Density of $N=200$ fermions obtained by direct numerical calculations (solid line), and one dimensional LDA (dashed line) at $\Omega/\omega_x = 0.9999$, and $\omega_y/\omega_x = 3.5$.

since the effective potential is not smooth along the strong confining direction. Thus we need a different approach to treat the density in this regime. The 1DLDA lead us to the semicircular profiles for the atoms along the weak trapping direction,

$$\rho(x, y = 0) = \rho(0, 0) \sqrt{1 - \frac{x^2}{L^2}}. \quad (2.64)$$

Here, L is the radius of the cloud and is defined by

$$L/l_x = \sqrt{\frac{2\mu/\hbar\omega_x - \omega_-/\omega_x}{1 - \tilde{\Omega}^2}}. \quad (2.65)$$

the results for the 1DLDA is shown in Fig. (2.9b), in which the approximation introduces the density profile in good agreement with the exact solution. The description nicely illustrates the density profiles for higher anisotropy values, but the Friedel oscillations are absent. The agreement in the density of the numerically calculated profiles from exact solutions and the one from 1DLDA support our interpretation of the sub-bands formed by the quantization in the strong trapping direction for highly anisotropic Landau levels.

2.2.3 Temperature effects

In order to add the effect of temperature we use the Fermi distribution function as we did in isotropic case. We recall Eq. (2.17) to calculate the density profiles at finite temperatures. Choosing the appropriate temperature values in our calculations, we investigate the effect of temperature on structure of profiles, which are shown in figure 2.10. We expect from isotropic case that the temperature around the gap between two landau levels, $k_B T \sim \hbar\omega_-$, smears out the step structure in two dimensional regime. However, in the case of one dimensional regime, a low temperature also cause changes in density of fermions. As soon as the temperature is turned on, Friedel oscillations are smeared out since the energy scale related to the Friedel oscillations is the small value of $\hbar\omega$. The higher temperature values make the density profiles more smooth. For both one and two dimensional regimes at room temperature a gaussian profile is observed, the structure that we expect from a Boltzmann gas.

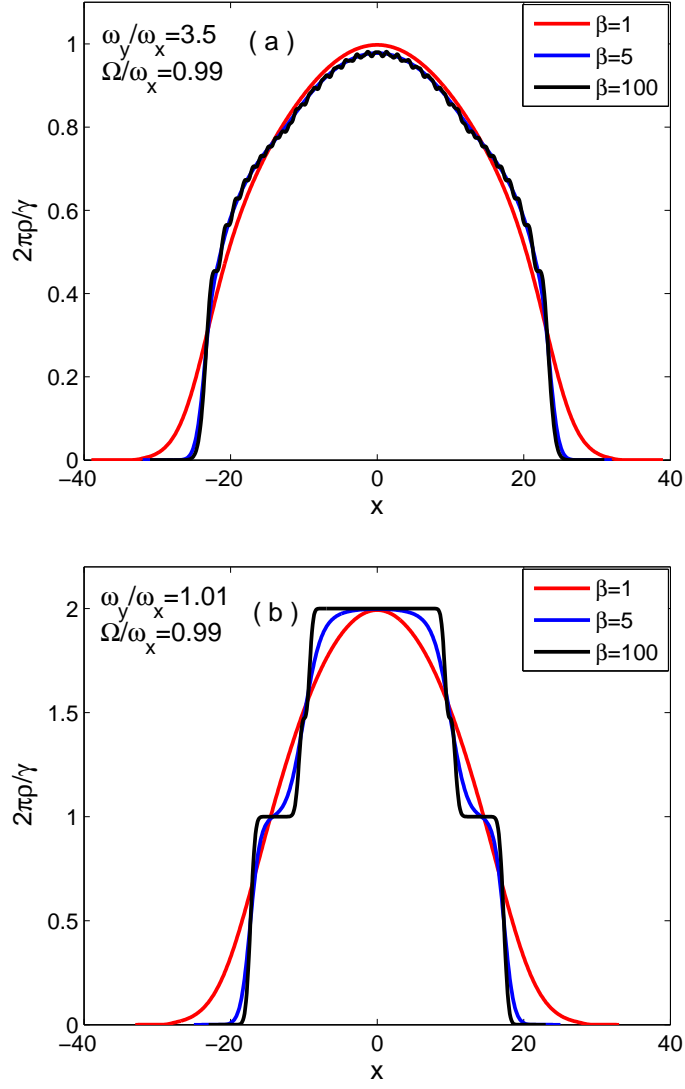


Figure 2.10: (a) Density profile for fermions at different temperatures and at $\Omega/\omega_x = 0.99$, and $\omega_y/\Omega_x = 3.5$. (b) Density profile for fermions at different temperatures and at $\Omega/\omega_x = 0.99$, and $\omega_y/\Omega_x = 1.01$. The oscillations (a) and the layered aspect of the profiles (b) are eliminated by temperature. Here $\beta = \frac{\hbar\omega_x}{k_b T}$ is the normalized inverse temperature.

CHAPTER 3

VORTEX LATTICES OF RAPIDLY ROTATING BOSE-EINSTEIN CONDENSATES

One of the most important properties of Bose-Einstein condensates is their response to the rotation. The rotation in Bose condensates gives rise to the existence of quantized vortices. An interesting property of vortices is their desire to form lattices when the rotation is fast enough, due to the interactions between atoms. The property that is also observed in superconductors with a lattice of magnetic quantized fluxes, called the Abrikosov lattice. In the case of a Bose condensate composed of atoms occupying the same hyperfine states (one component Bose gas), the lattice is the same as the Abrikosov lattice for superconductors [36], which is known to be a hexagonal lattice [82]. However, the number of components as well as the quality and sort of the interactions introduce new types of vortex lattices [37, 38, 39]. Then it will be helpful to study the effect of interactions on vortex lattice in the limit of fast rotation. The effect of interactions are not only limited to the creation of new type of vortices, but it is also known that the inter-particle interactions play an important role in stability and dynamics of the condensates [11, 32].

Another feature of ultracold atoms that enriches this field is the existence of relatively strong long range dipolar interaction. The magnetic moment of condensates of alkali atoms is very weak ($\mu = 1\mu_B$) with respect to the contact interaction. However, the magnetic trapping of atomic chromium [83], which has higher magnetic moment ($\mu = 6\mu_B$), and then observation of Bose-Einstein condensation of chromium [84] caused new experimental and theoretical efforts in this field. The long range character of this interaction also opens new horizons for researchers in the investigation of

different quantum phases. Based on these facts, along with the researches on general properties of the dipolar condensates, such as ground state [85], dynamics [86], and stability [87, 88, 89], the investigations on realization and control of different quantum phases in condensates with dipolar bosons [90, 91] are at the center of attention.

The effects of interactions on vortex lattices in rotating Bose gases have also been investigated extensively [36, 37, 38, 39]. It is now well known that the formation of different lattice types depends on the strength of interactions between particles. New types of vortex lattices have been found as a result of interactions between atoms [37, 38], and researchers are still seeking new types of lattices.

The properties of the single and two component rotating Bose-Einstein gases have been studied analytically by Ho and Mueller [36, 37]. They show that the vortex lattices differ under s-wave interaction and also new types of lattices rather than the triangular lattice are determined because of this interaction between like and unlike atoms. The method developed in [37] has been successfully used to investigate the excitations [92], dipolar condensates [38], and also more complicated Bose systems [93]. It is shown in [38] that the dipolar interaction along with s-wave interaction also result in a new vortex lattice for one component Bose-Einstein condensate. Drastic changes caused by dipolar interactions in fast rotating condensates [38, 39] motivated us to study multi-component condensates with dipolar interactions.

In this chapter, the vortex lattice structures of two component Bose-Einstein condensates with magnetic dipole-dipole interaction in the limit of large number of vortices are investigated. The details of the method used to determine the type of vortex lattices are given in the next section. Finally, a phase diagram which describes the structure of lattices in terms of long-range dipolar interaction and short-range contact interaction strength is presented. The detailed discussions of the different phases and also the limits of single component with dipolar interaction [38] and two component gas without dipolar interaction [37] are also given in this chapter.

3.1 Mean field quantum Hall regime

The first attempts to understand the physics of rapidly rotating ultracold atoms revealed the connection between very fast rotating atomic gas and quantum Hall effect [30, 31]. The description was implied to a Bose-Einstein condensates with large number of vortices by Ho [36]. The importance of this regime is that the system is exactly solvable in this limit which allows one to do the calculations analytically. In this section we will review in detail the properties of condensates in quantum Hall regime which is mainly carried out in [36].

We first consider a system of Bose-Einstein condensate in a three dimensional harmonic trap. The system can be described by the Gross-Pitaevskii energy functional which gives the wavefunction of the condensate, when the total number of particles is constant. Thus we need to write the energy functional for the condensate in an isotropic harmonic trap with a frequency of ω , and rotating at angular frequency Ω around z axis

$$E[\Psi(x)] = \int d^3x \Psi^*(x) \left[\frac{P^2}{2M} + \frac{1}{2} M \omega^2 R^2 - \Omega L_z \right] \Psi(x) + \frac{1}{2} g \int d^3x |\Psi(x)|^4, \quad (3.1)$$

where \mathbf{R} and \mathbf{P} are three dimensional position and momentum operators, respectively. Before starting the minimization of the energy functional with the given condition it is useful to explore some important properties of the system. The main feature of this system is the similarity between the Hamiltonian of the rotating particles in a trap and a two dimensional electron gas subjected to a strong uniform magnetic field. The single particle Hamiltonian appearing in the first integral of energy functional can be expressed in a different way to see this similarity in more explicit form.

$$\begin{aligned} H &= \frac{P^2}{2M} + \frac{1}{2} M \omega^2 R^2 - \Omega L_z \\ &= \frac{1}{2M} (\mathbf{p} - M \boldsymbol{\Omega} \times \mathbf{r})^2 + \frac{1}{2} M (\omega^2 - \Omega^2) r^2 + \frac{p_z^2}{2M} + \frac{1}{2} M \omega^2 z^2. \end{aligned} \quad (3.2)$$

Here $\mathbf{p} = (p_x, p_y)$, $\mathbf{r} = (x, y)$, M is the mass of the particle, and L_z is the angular momentum in the z direction. The equivalence of two systems is obviously seen in the second form of the Hamiltonian, which describes a charged particle, q , in an effective magnetic field with a vector potential of $\mathbf{A} = \frac{M}{q} \boldsymbol{\Omega} \times \mathbf{r}$. This part of the Hamiltonian can be diagonalized applying two successive canonical transformations,

which is shown in chapter 2 in detail. The energy eigenvalues of the system can be found which have the form

$$E_{mn} = \hbar(\omega + \Omega)n + \hbar(\omega - \Omega)m + \hbar\omega, \quad (3.3)$$

where $n \geq 0$ labels the Landau levels and $m \geq 0$ counts the sublevels in each Landau level. The corresponding eigenfunctions of the system are introduced in Eq. (2.7).

In the limit of very fast rotation i.e. $\omega - \Omega$ is very small in Eq. (3.3), one can easily see that two successive Landau levels are separated by $2\hbar\omega$. Moreover, in this limit the centrifugal force $M\Omega^2 r$ nearly cancels the trapping force $M\omega^2 r$. As a result, the condensate almost becomes a flat cloud. The area occupied by the atoms increases which gives a smaller density n for the system [94]. A smaller density means a smaller interaction term and when the rotation is fast enough, or correspondingly when the interaction energy is sufficiently small $gn \ll \hbar\omega$, the system fills now the highly degenerate $n = 0$ level, the well known LLL [30, 31, 36]. Abrikosov shows that the wavefunction in this limit can be written as a linear combination of single particle eigenfunctions, $\psi_{0m} = \psi_m$ [95]. Then for an assembly of cold identical bosons rotating at frequency Ω ,

$$\begin{aligned} \Psi(r) &= \sum_m c_m \psi_m \\ &= \sum_m c_m u^m \exp\left[\frac{-r^2}{2a}\right] \\ &= f(u) \exp\left[\frac{-r^2}{2a}\right]. \end{aligned} \quad (3.4)$$

Here $f(u)$ is a polynomial (an analytical function of u), and $u = x + iy$.

The LLL description of the Bose-Einstein condensation in fast rotation provides the groundwork to study the vortex structures of condensates analytically. The polynomial in the wavefunction can be written in accordance with the fundamental theorem of algebra as

$$f(u) = \prod_i^m (u - u_i), \quad (3.5)$$

where u_i 's are the zeros of the polynomial. These zeros are the position for the vortices as f shows a phase change of 2π when u encircling u_i , since they are complex variables. It is supposed that the zeros of Ψ which are the zeros of $f(u)$ form an infi-

nite lattice. Our task is to find the structure of the vortex lattices which minimize the energy functional with respect to wavefunction Ψ .

3.2 Vortex lattices of dipolar two component Bose-Einstein condensates

In this section, we consider a disk-shape two component Bose-Einstein condensate with contact and dipolar interactions, which is subjected to rapid rotation. Each component can be considered as a different hyperfine state of the same atom. The trap geometry is important in determining the nature of interaction. For disk shape condensates the atoms are settled side by side, additionally we assume that the magnetic dipoles are aligned in the same direction. Thus the dipole-dipole interaction between atoms is repulsive. The vortex structures are calculated by minimizing the energy based on works done by Ho and Mueller [36, 37]. By changing the strength of the interactions we observe that the vortex lattices go through different structural phase transitions. Since the system is subjected to two different interactions, it is difficult to interpret the effect of interaction on vortex structure. However the results of works done in [37, 38] makes the interpretation a little bit easier. We show that the results give the vortex structures in the limit of the two component regime studied in [37] and one component regime with dipolar interaction handled in [38].

We consider that the components of the condensate are described with a wave function Ψ_i , where $i = 1, 2$. The condensate is rotated at a fixed rotation frequency Ω , which is fast enough to consider the mean field quantum Hall regime. The Gross-Pitaevskii energy functional of the system is:

$$E[\Psi] = \sum_{i=1,2} \int d^2r \Psi_i^* \left[\frac{-\hbar^2}{2M} \nabla^2 + \frac{1}{2} m \omega^2 r^2 - \Omega L_z \right] \Psi_i + E_s + E_d, \quad (3.6)$$

where L_z is the angular momentum along the rotation direction, and E_s and E_d are the scattering and dipolar interaction energies, respectively. These energies are defined

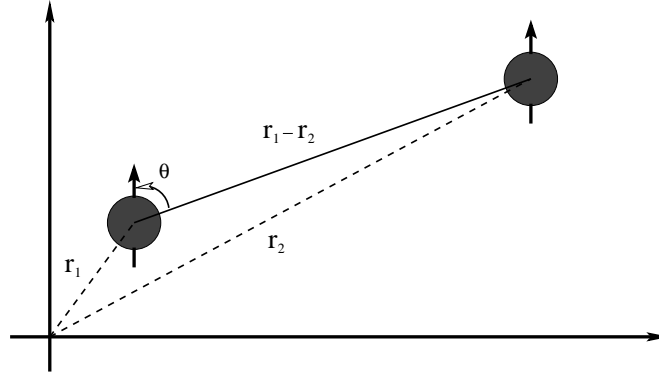


Figure 3.1: Dipole-dipole interaction.

as

$$\begin{aligned}
 E_s &= \frac{1}{2} \sum_{i=1,2} g_i \int d^2r |\Psi_i|^4 + g_{12} \int d^2r |\Psi_1|^2 |\Psi_2|^2, \\
 E_d &= \sum_{i=1,2} \mu_i^2 \int dr_1 dr_2 |\Psi_i(r_1)|^2 V(\mathbf{r}_1 - \mathbf{r}_2) |\Psi_i(r_2)|^2 \\
 &\quad + \mu_1 \mu_2 \int dr_1 dr_2 |\Psi_1(r_1)|^2 V(\mathbf{r}_1 - \mathbf{r}_2) |\Psi_2(r_2)|^2,
 \end{aligned} \tag{3.7}$$

where $g_i = 4\pi\hbar^2 a_i/M$ and $g_{12} = 4\pi\hbar^2 a_{12}/M$ are the s-wave interaction coupling constants between like and unlike atoms, respectively, and μ_i 's are the magnitudes of magnetic dipole moment of each component. The magnetic dipole-dipole interaction is given by expression

$$V(r_1 - r_2) = -\frac{\mu_0}{4\pi} \frac{3(\mathbf{m}_1 \cdot \mathbf{e}_1)(\mathbf{m}_2 \cdot \mathbf{e}_2) - \mathbf{m}_1 \cdot \mathbf{m}_2}{|\mathbf{r}_1 - \mathbf{r}_2|^3}, \tag{3.8}$$

where \mathbf{m}_1 and \mathbf{m}_2 are unit vectors in the direction of magnetic dipoles μ_1 and μ_2 . Here \mathbf{e}_1 and \mathbf{e}_2 are the unit vectors parallel to \mathbf{r}_{12} , the line joining the centers of the two dipoles. Figure 3.1 illustrates the picture explicitly. Here we assume that the magnetic dipoles are parallel to each other, and perpendicular to \mathbf{r}_{12} . In this case the magnetic dipole interaction has a simple expression given by

$$V(r_1 - r_2) = \frac{\mu_0}{4\pi} \frac{1}{|\mathbf{r}_1 - \mathbf{r}_2|^3}. \tag{3.9}$$

The wavefunction of each component is normalized such that

$$\int d^2r |\Psi_i|^2 = N_i, \quad (3.10)$$

where we assume that the densities for both components are equal. Moreover, we assume that for the s-wave interactions $g_1 = g_2 \neq g_{12}$, and for the dipolar interactions $\mu_1 = \mu_2$. For a two component Bose gas in which both components are subjected to the same rotation frequency, vortex lattices have the same structure, but one is shifted with respect to another. Then the wavefunctions for both components can be introduced by two basis vectors and one relative displacement vector. We assume that the \mathbf{B}_1 and \mathbf{B}_2 are the basis vectors of the infinite lattice, and \mathbf{r}_0 is the relative displacement of the vortices of different kind. The area of the unit cell is

$$v_c = |\mathbf{B}_1 \times \mathbf{B}_2|. \quad (3.11)$$

It is shown that that $|\Psi(r)|^2$ can be written as a product of a gaussian and a function $g(r)$ which is periodic under lattice transformation [36]

$$|\Psi(r)|^2 = A e^{\frac{-r^2}{\sigma^2}} g(r). \quad (3.12)$$

Here σ is related to the number of the vortices and is given by

$$\frac{1}{\sigma^2} = \frac{1}{a^2} - \frac{\pi}{v_c}. \quad (3.13)$$

Using Fourier transform, $g(r)$ is written as

$$g(r) = \frac{1}{v_c} \sum_K g_K e^{i\mathbf{K} \cdot \mathbf{r}}, \quad (3.14)$$

where \mathbf{K} 's are the reciprocal lattice vectors. From the normalization of Ψ one can obtain

$$|\Psi_1|^2 = \frac{1}{\pi\sigma^2} \sum_K \tilde{g}_K e^{i\mathbf{K} \cdot \mathbf{r}} e^{\frac{-r^2}{\sigma^2}}, \quad (3.15)$$

$$|\Psi_2|^2 = \frac{1}{\pi\sigma^2} \sum_K \tilde{g}_K e^{i\mathbf{K} \cdot (\mathbf{r} - \mathbf{r}_0)} e^{\frac{-r^2}{\sigma^2}}, \quad (3.16)$$

$$\tilde{g}_K = \frac{g_K}{\sum_{K'} g_{K'} e^{\frac{-\sigma^2 K'^2}{4}}}. \quad (3.17)$$

The presence of $|\Psi|^4$ and $|\Psi_1|^2 |\Psi_2|^2$ in the energy function leads to the definition of quantities

$$\begin{aligned} I &= \pi\sigma^2 \int d^2r |\Psi_i|^4 \\ I_{12} &= \pi\sigma \int d^2r |\Psi_1|^2 |\Psi_2|^2, \end{aligned} \quad (3.18)$$

to write the energy in a more compact form. One can obtain I 's using the expression for $|\Psi_i|^2$'s

$$I = \sum_{K,K'} \tilde{g}_K \tilde{g}_{K'} e^{\frac{-\sigma^2 |K+K'|^2}{4}}, \quad (3.19)$$

$$I_{12} = \sum_{K,K'} \tilde{g}_K \tilde{g}_{K'} e^{-iK \cdot r_0} e^{\frac{-\sigma^2 |K+K'|^2}{4}}. \quad (3.20)$$

To obtain the lattice types we need to minimize the energy functional with respect to lattice basis vectors. Thus we need to express g_K 's in terms of the length of the basis vectors. In order to obtain such expressions we introduce a complex representation for the basis vectors, $b_i = (\hat{\mathbf{x}} + i\hat{\mathbf{y}}) \cdot \mathbf{B}_i$. If we choose the lattice vectors such that \mathbf{B}_1 lies on the x-axis, then b_1 will be real

$$\mathbf{B}_1 = b_1 \hat{\mathbf{x}} \quad , \quad \mathbf{B}_2 = b_1(u\hat{\mathbf{x}} + v\hat{\mathbf{y}}), \quad (3.21)$$

$$b_2 = b_1(u + iv), \quad (3.22)$$

Then the area of the unit cell is

$$v_c = |\mathbf{B}_1 \times \mathbf{B}_2| = b_1^2 v. \quad (3.23)$$

We substitute the periodic part of the wavefunction with the Jacobi theta function which has the exact zeros of the analytical function $f(u)$

$$f(u) = \Theta(\zeta, \tau) e^{\pi u^2 / 2v_c}, \quad (3.24)$$

where $\zeta = u/b_1$ and $\tau = b_2/b_1$. Using the expression for the theta function the Fourier coefficients are derived to be [37]

$$g_K = (-1)^{m_1+m_2+m_1m_2} e^{\frac{-v_c |K|^2}{8\pi}} \sqrt{\frac{v_c}{2}},$$

$$v_c K^2 = \left(\frac{2\pi}{v} \right) \left[(vm_1)^2 + (m_2 - um_1)^2 \right], \quad (3.25)$$

where $\mathbf{K} = m_1 \mathbf{K}_1 + m_2 \mathbf{K}_2$, and m_1 and m_2 are integers. Here \mathbf{K}_1 , and \mathbf{K}_2 are the basis vectors of the reciprocal lattice and are given by

$$\begin{aligned} \mathbf{K}_1 &= \frac{2\pi}{v_c} \mathbf{B}_2 \times \mathbf{z} \\ \mathbf{K}_2 &= \frac{2\pi}{v_c} \mathbf{z} \times \mathbf{B}_1. \end{aligned} \quad (3.26)$$

Noting that we deal with a large number of vortices, the expression for I and I_{12} take more simple forms of

$$I = \sum_K \left| \frac{g_K}{g_0} \right|^2, \quad I_{12} = \sum_K \left| \frac{g_K}{g_0} \right|^2 \cos \mathbf{K} \cdot \mathbf{r}_0. \quad (3.27)$$

The s-wave interaction energy then has the form

$$E_s = \frac{gn^2}{\pi\sigma^2} \left(I + \frac{g_{12}}{g} I_{12} \right). \quad (3.28)$$

Following similar steps for the dipolar part of the energy expression, and also assuming that $\mu_1 = \mu_2 = \mu$, we obtain

$$\begin{aligned} E_d &= \frac{\mu_0\mu^2}{4\pi} \frac{n^2}{(\pi\sigma^2)^2} \sum_K \left| \frac{g_K}{g_0} \right|^2 (1 + \cos \mathbf{K} \cdot \mathbf{r}_0) \\ &\times \int d^2r_1 d^2r_2 e^{i\mathbf{K} \cdot (\mathbf{r}_2 - \mathbf{r}_1)} \frac{e^{-\frac{(r_1+r_2)^2}{\sigma^2}}}{|\mathbf{r}_1 - \mathbf{r}_2|^3}. \end{aligned} \quad (3.29)$$

We do a transformation to the center of mass coordinates, writing the dipole interaction energy in terms of the relative displacement $\mathbf{r} = \mathbf{r}_2 - \mathbf{r}_1$ and center of mass coordinate $2R = r_1 + r_2$, then integrating with respect to \mathbf{R} we have

$$E_d = \frac{n^2\mu_0\mu^2}{8\pi^2\sigma^2} \sum_K \left| \frac{g_K}{g_0} \right|^2 (1 + \cos \mathbf{K} \cdot \mathbf{r}_0) \int d^2r \frac{e^{i\mathbf{K} \cdot \mathbf{r}_0}}{r^3} e^{-r^2/2\sigma^2}. \quad (3.30)$$

This leads to a radial integral for the energy expression as

$$E_d = \frac{n^2\mu_0\mu^2}{4\pi\sigma^2} \sum_K \left| \frac{g_K}{g_0} \right|^2 (1 + \cos \mathbf{K} \cdot \mathbf{r}_0) \int_0^\infty dr \frac{1}{r^2} [J_0(Kr) e^{-r^2/2\sigma^2}]. \quad (3.31)$$

There is a problem in evaluating the integral with respect to r when it approaches zero. To solve this problem we define a cutoff Λ and write the integral as

$$\begin{aligned} E_d &= \frac{n^2\mu_0\mu^2}{4\pi\sigma^2} \sum_K \left| \frac{g_K}{g_0} \right|^2 (1 + \cos \mathbf{K} \cdot \mathbf{r}_0) \\ &\times \left\{ \frac{1}{\Lambda} + \int_0^\infty dr \frac{1}{r^2} [J_0(Kr) e^{-r^2/2\sigma^2} - 1] \right\}. \end{aligned} \quad (3.32)$$

Since we work in the limit of the large number of the vortices, we can neglect the gaussian term and make a change of variables to write the expression in a simple form

$$E_d = \frac{n^2\mu_0\mu^2}{4\pi\sigma^2} \sum_K \left| \frac{g_K}{g_0} \right|^2 (1 + \cos \mathbf{K} \cdot \mathbf{r}_0) \left\{ \frac{1}{\Lambda} + K \int_0^\infty \frac{dx}{x^2} [J_0(x) - 1] \right\} \quad (3.33)$$

with an integral appearing in the energy expression, which is only equal to -1 . Then, the full interaction energy can be written as

$$E_{int} = \frac{n^2 \mu_0 \mu^2}{4\pi \sigma^2 a} [\alpha I + \beta I_{12} - D], \quad (3.34)$$

where

$$\begin{aligned} D &= \sum_{\mathbf{K}} \left| \frac{g_{\mathbf{K}}}{g_0} \right|^2 K a (1 + \cos \mathbf{K} \cdot \mathbf{r}_0) \\ \alpha &= \frac{4ga}{\mu_0 \mu^2} + \frac{a}{\Lambda} \\ \beta &= \frac{4g_{12}a}{\mu_0 \mu^2} + \frac{a}{\Lambda}. \end{aligned} \quad (3.35)$$

3.2.1 Vortex pattern

We obtain a variety of vortex lattice types as a function of parameters α and β by minimizing the energy in Eq.(3.34) numerically. The lattices are determined in the unit of basis vectors \mathbf{B}_1 and \mathbf{B}_2 and also $\mathbf{r}_0 = a\mathbf{B}_1 + b\mathbf{B}_2$. Lattice structures can be specified in terms of aspect ratio τ and lattice angle θ such that $u + iv = \tau e^{i\theta}$. We introduce a phase diagram for the lattice types as a function of the α and β in Fig. (3.2). The new types of vortex lattices are obtained which can be described as overlapped square and overlapped rectangular lattices. We expect that the phase diagram includes the lattice types for two component Bose gas studied in [37] when the dipolar interaction vanishes, and also the regime for the single component Bose gas with dipolar interaction studied in [38], when we ignore the differences between atoms of different species.

Since dipole-dipole interaction is the same between like and unlike atoms, in the energy expression Eq. (3.34) α , and β can be interpreted as the energy contribution for intra-component and inter-component interaction, respectively. The α part contains g , thus it dominantly governs the behavior of each component inside. Since α could be negative, it is important in the collapse of the condensate. It is known that the condensate may collapse for strong attractive interaction. The β part which contains g_{12} , determines the behavior of the two components with respect to each other. Although the third part, i.e. D , is positive definite, with its minus sign in the expression there is always an attractive part inside the energy.

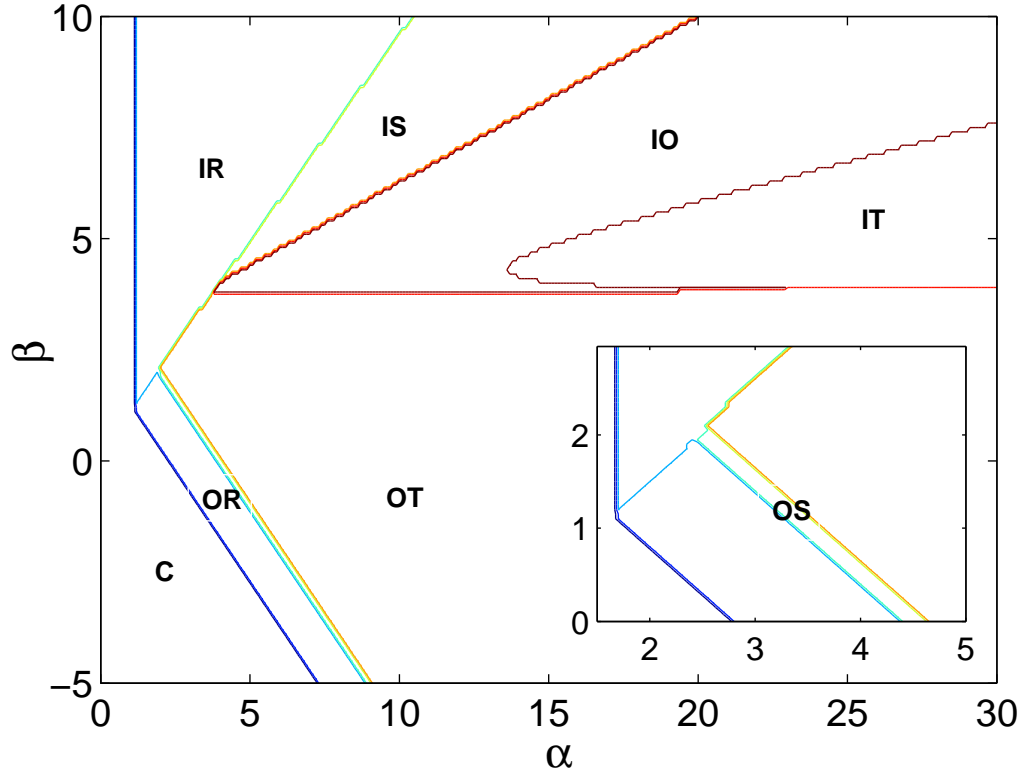


Figure 3.2: Phase diagram showing lattice structures for different values of interaction terms α , and β . Here, C corresponds to collapse region, and IR, IS, IO, IT, OR, OT, and OS stand for interlaced rectangular, interlaced square, interlaced oblique, interlaced triangle, overlapped rectangular, overlapped triangle, and overlapped square, respectively. The inset figure indicates the region for overlapped square lattices, a new type of lattice structure for rotating Bose condensates.

Adjusting the strength of parameters α , and β , also enables us to control the switching between the regime of dominated dipolar condensate and the regime of ordinary two component condensate. One can easily conclude from Eq. (3.34) that for small values of α and β the dipole-dipole interaction is the dominant part, however for large values of α and β , the contact interaction dominates.

For large α , and β , the last term D can be ignored and lattice structures are determined by their ratio. Thus the work reduces to the minimization of the term

$$J = I + \frac{\beta}{\alpha} I_{12}. \quad (3.36)$$

The behavior is similar to ordinary two component BEC energy expression introduced in [37] (see figure 3.3a).

In the case of the dipole-dominant regime and when $g = g_{12}$, the two component gas behaves like a one component gas. Thus the problem reduces exactly to the system studied in [38] for which the interaction energy is

$$E_{int} = \frac{n^2 \mu_0 \mu^2}{2\pi \sigma^2 a} [\alpha I - D]. \quad (3.37)$$

For this case we obtained the vortex structures introduced in [38] (see figure 3.3b). The detailed analysis of the different aspects of introduced phase diagram is given in the following parts.

- i) The dominant attractive interaction causes the condensate to collapse for $\alpha < 1.25$. The condensate collapses even for large β values, since it is not an important factor in determining the stability of each component inside.
- ii) For $\alpha > 1.25$, and $\beta < 1.25$, the inter-component attraction is strong enough to overcome the dipolar repulsion between unlike atoms which result in overlapped lattices. By increasing α , the vortex structures undergo structural phase transition from overlapped rectangular to overlapped square lattice and then to overlapped triangular lattices since α values, as α is the dominant part in determining the lattice structures for each component.
- iii) For $1.25 < \alpha < 3.70$ and $1.25 < \beta < 3.70$; the comparison of these two parameters determines the position of lattice points of one species with respect to another species.

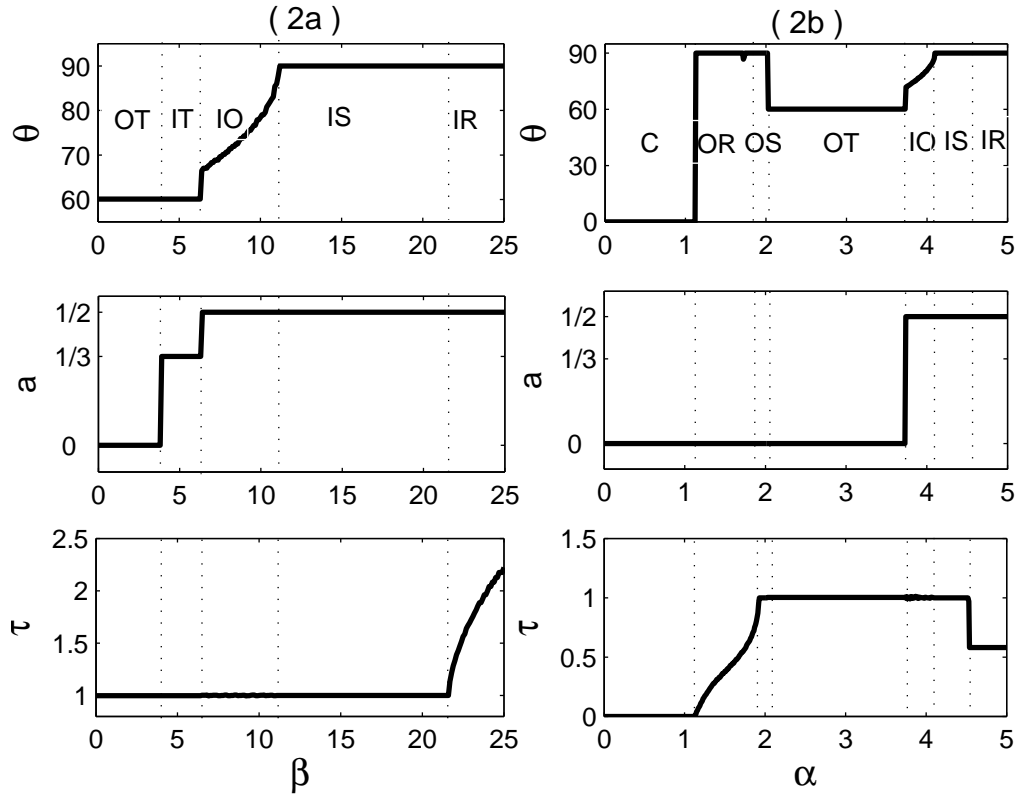


Figure 3.3: The parameters indicating the type of lattice structures as a function of interaction interaction terms α , and β . The phase diagram is reduced to different regimes: (a) The limit for ordinary two component condensate. (b) The limit for dipolar single component condensate. Here τ and, θ are the lattice parameters and define the lattice structure, and a , indicates the displacement of the lattice structures of one species with respect to another species.

In this region, when $\alpha < \beta$ interlaced rectangular lattice forms. On the other hand, when $\alpha > \beta$, overlapped lattice form.

iv) When $\alpha \geq 3.70$ and $\beta \geq 3.70$, only interlaced lattices exist in the phase diagram. This is an expected result as inter-component interaction is not attractive any more. The repulsive forces between two different species cause the minima of one type to move to maxima of another type. In this region by increasing α the structures of the lattices changes from interlaced rectangular to interlaced square, oblique, and finally triangle lattices.

We expect that the phase diagram to also cover two regimes studied in [37, 38]. For such limits, two different cut lines can be taken on the phase diagram; $\alpha = \text{constant}$ line, and $\alpha = \beta$ line, which are expected to give the ordinary two component, and single component dipolar condensates, respectively. Note that if we fix α and change β , it corresponds to the variation of g_{12} , and $\alpha = \beta$ means that $g = g_{12}$ and as dipolar interaction exists the situation is like one component condensate with dipolar interaction. Minimization along these lines is shown in Fig. (3.3).

In the case of ordinary two component limit, the cut line gives us all the phases observed in [37] (see figure 3.3a). The interlaced rectangular, square, oblique, and triangle and overlapped triangle lattices are obtained for this part. When $\alpha = \beta$ also we observe the same vortex lattices which have been determined for the single component Bose gas with dipolar interactions (see figure 3.3b). The results for this case are a little complicated, then we illustrate them in a more explicit manner

a) $\alpha > 4.54$: In this region, the triangle vortex lattices are observed, but it is not easily seen in the figure. The two component gas forms interlaced rectangular lattices, but the combined lattices form triangular lattice together when one ignores the difference between unlike species, as $g = g_{12}$. It is easy to observe this in figure 3.4 for IR (interlaced rectangular) lattices.

b) $4.1 < \alpha < 4.54$: In this region, square lattices are observed. The atoms of both gases form interlace square lattices and when the atoms are taken to be same the combined lattices again form square lattices.

c) $3.73 < \alpha < 4.1$: In this region, the resulted vortex lattices are determined to be rectangular under dipolar interaction. The two component gas forms interlace oblique

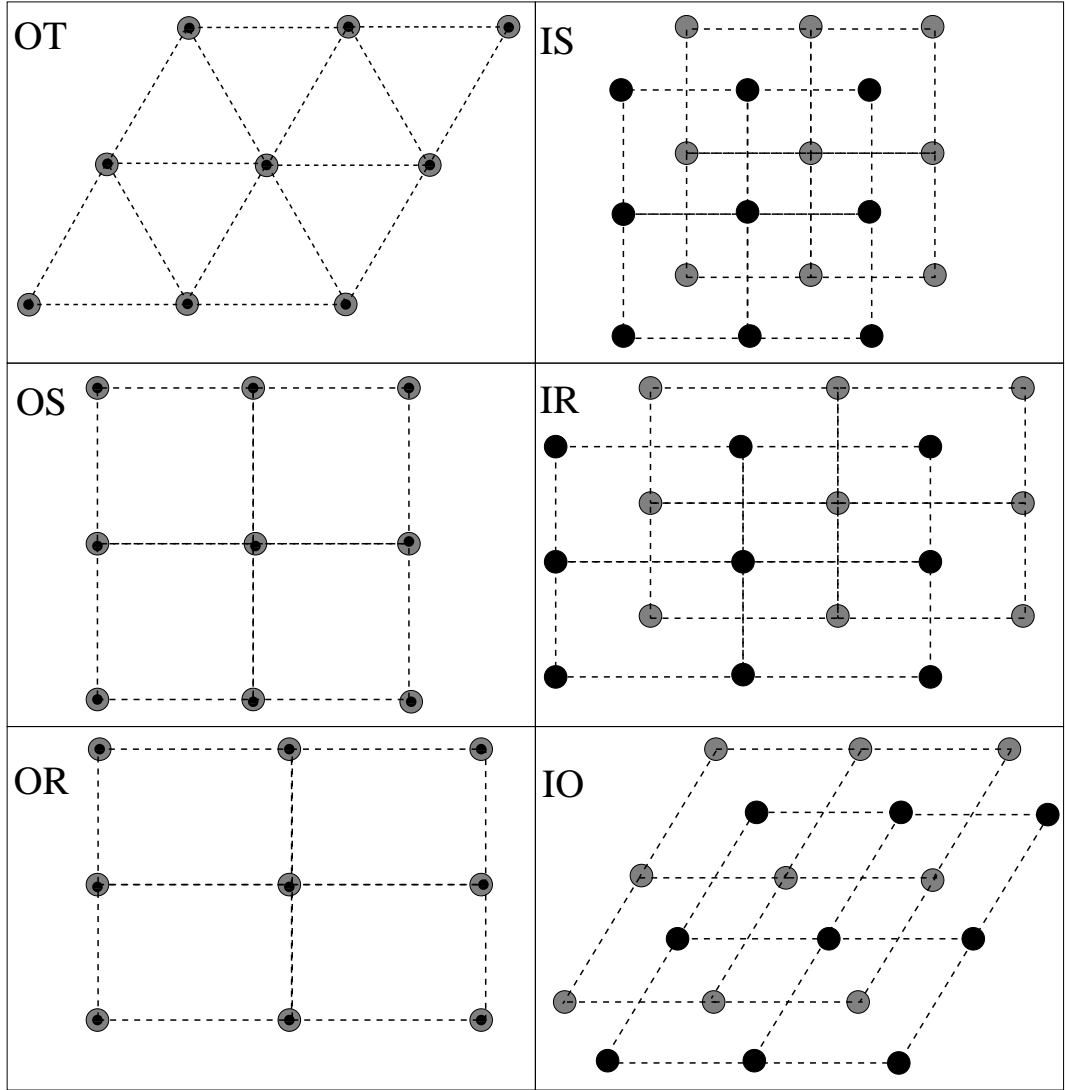


Figure 3.4: Lattice structures for dipolar two component condensates. Black and gray dots corresponds to vortices of two condensates.

lattices but the combined lattices form rectangular lattices when the atoms are taken to be the same. This lattices also are clearly seen in figure 3.4 for IO lattices.

d) $2.02 < \alpha < 3.73$: Since the lattice structure for two component condensate is overlapped triangles in this region, the combined lattices are also triangular.

e) $1.92 < \alpha < 2.02$: In this region square lattices are formed when the differences between species are ignored. The lattice structure for two component gas is overlapped square.

f) $1.12 < \alpha < 2.02$: The resulted lattices are determined to be rectangular, as the original lattices are also overlapped rectangular in the case of two component dipolar gas.

g) $\alpha < 1.12$: In this region condensate collapses.

CHAPTER 4

SUMMARY AND CONCLUSION

In this study we investigate the properties of trapped atoms subjected to rapid rotations. The study is divided into two distinct parts, one for fermions another for bosons. In the case of a Fermi gas we explore the density structure of non-interaction cold atoms when are rotated rapidly. on the other hand, for rapidly rotating Bose condensate, we search for new lattice structures in the presence of contact and dipolar interactions.

First, The density structure of Fermi gases in a rotating traps are investigated. We focus on anisotropic trap case, in which two distinct regimes depending on rotation frequency and anisotropy are observed. Two regimes can be illustrated by a simple description of maximum number of states between two Landau levels, which are separated from each other by a minimum point, ω_{yc} in the this description. For small anisotropy values, when $\omega_y \ll \omega_{yc}$, the density profiles show a step structure each step is demonstrated by an elliptical plateaus. Each plateau represents a Landau level with a constant density. The local density approximation describe the two dimensional regime with a perfect similarity in structure of fermion density. The case for one dimensional regime is a little different from the two dimensional case. For large anisotropy values, $\omega_y \gg \omega_{yc}$, the Friedel oscillation is the dominant aspect of the density profiles. The density profiles show gaussian structure along the direction of strong trapping, with a semicircular forms with prominent oscillations along weak confining direction. Again, the system is nicely described by local density approximation in this regime. A smooth crossover between two regimes is observed, with a switching from a step structure profile to a soft edge transition with Friedel oscillation. At finite temperatures, the step structure are smeared out in two dimension. In

one dimensional regime the Friedel oscillations are cleaned as soon as the temperature is turned on.

The smooth switching between two regimes is present in the nature of the wavefunctions for the rotating anisotropic trap. Such smooth transition provides a mapping between states of two dimensional system to the one dimensional system. The study can be extended to the case of interaction Fermi, or even Bose gases to investigate the properties of states in an extremely elongated trap.

The cooling of fermions during the experiments is one of the major difficulties in the study of cold Fermi gases in the labs, since the fermionic atoms are non-interaction [60, 61, 62, 63, 64, 65]. However, the observation of some properties, like step structure of fermion in rotating traps is within the capability of current experiments. The other issue about the experimental possibility of our system is the usual use of isotropic traps for cooling and rotating atoms. nevertheless, the implementation of the rotating process with anisotropic trap [69], lights the hopes of experimental demonstration of the system discussed in this study.

The density profile measurements are carried out by the method of expansion imaging. This method enable us to observe the main aspects of the density profiles such as the step structure of two dimensional rotating Fermi gas or the semicircular profile of a fermionic gas in a rotating highly anisotropic trap. However, the more detailed features, such Friedel oscillations needs a more complicated methods such as Bragg spectroscopy [96].

It also worth to remark that the addition of the interaction to the system would be interesting. Specially, the presence of relatively strong dipole-dipole interaction in some atomic gases [84] makes it more favorable to study the effect of such interaction on the density profiles.

The second part of the study is devoted to the investigation of different lattice structures in two component Bose condensates subjected to very fast rotation, this time in the presence of interactions. The bosonic atomic gases enjoy the presence of contact interactions. Moreover, the observation of dipole-dipole interaction in atomic gases [84] improves the richness of the system.

We explore the existence of new vortex lattice structures for dipolar two component condensates scanning a wide range of interaction strengths. We introduce a phase diagram as a function of intra and inter-component interactions showing different type of vortex lattice structures. New type of lattice structures, overlapped square and overlapped rectangular, are determined as a result of dipolar interactions and s-wave interaction for two component condensate. The region where the attractive inter-component interactions dominates the repulsive once, the overlapped lattices are formed. The intra-component interactions, which defines the behavior of each component inside, results in different type of lattices by changing the strength of interactions.

Two different limits of phase diagram reproduce the results of ordinary two component and dipolar one component Bose condensates. Ordinary two component condensate are produced by fixing intra-component s-wave interactions for a constant value of dipole moment, and changing inter-component s-wave interaction. The dipolar one component condensate is obtained by equalizing intra and inter-component s-wave interaction, which enable us to get rid of differences between like and unlike atoms. The results of calculation are in agreement with the results of previous studies for two regimes [37, 38].

REFERENCES

- [1] S. N. Bose, Z. Phys. Rev. **26**, 178 (1924).
- [2] A. Einstein, Sitzber. Kgl. Preuss. Akad. Wiss., **261** (1924).
- [3] A. Einstein, Sitzber. Kgl. Preuss. Akad. Wiss., **3** (1925).
- [4] M. H. Anderson, J. R. Ensher, M.R. Matthews, C. E. Wienman, and E. A. Cornell, Science **269**, 198 (1995).
- [5] K. B. Davis, M. O. Mewes, M. R. Andrews, N. J. van Druten, D. S. Durfee, D. M. Kurn, and W. Ketterle, Phys. Rev. Lett. **75**, 3969 (1995).
- [6] C. C. Bradley, C.A. Sackett, J. J. Tollett, and R. G. Hulet, Phys. Rev. Lett. **75**, 1687 (1995).
- [7] F. Dalfavo, S. Giorgini, L. P. Pitaevskii, S. Stringari, Rev. Mod. Phys. **71**, 463 (1999).
- [8] E. P. Gross, Nuovo Cimento **20**, 454(1961).
- [9] E. P. Gross, J. Math. Phys. **4**, 195 (1963).
- [10] L. P. Pitaevskii, Zh. Eksp. Teor. Fiz. 40, 646 (1961) [Sov. Phys. JETP **13**, 451 (1961)].
- [11] L. P. Pitaevskii, and S. Stringari, Bose-Einstein Condensation, Oxford University Press, Oxford (2003).
- [12] I. Bloch, J. Dalibard, and W. Zwerger, Rev. Mod. Phys. **80**, 885 (2008).
- [13] E. Tiesinga, B. J. Verhaar, and H. T. C. Stoof, Phys. Rev. A **47**, 4114 (1993).
- [14] S. Inouye, M. Andrews, J. Stenger, H. J. Miesner, S. Stamper-Kurn, and W. Ketterle, Nature **392**, 151 (1998).
- [15] P. Courteille, R. Freeland, D. Heinzen, F. van Abeelen, and B. Verhaar, Phys. Rev. Lett. **81**, 69 (1998).
- [16] M. Hafezi, A. S. Sorensen, E. Demler, and M. D. Lukin, Phys. Rev. A **76**, 023613 (2007).
- [17] K. Osterloh, N. Barberan, and M. Lewenstein, Phys. Rev. Lett. **99**, 160403 (2007).
- [18] B. Chung, and Th. Jolicoeur, Phys. Rev. A, **77**, 043608 (2008).
- [19] M. Olshanii, Phys. Rev. Lett. **81**, 938 (1998).

- [20] D. S. Petrov, G. V. Shlyapnikov, and J. T. M. Walraven, *Phys. Rev. Lett.* **85**, 3745 (2000).
- [21] D. Jaksch, C. Bruder, J. I. Cirac, C. W. Gardiner, and P. Zoller, *Phys. Rev. Lett.* **81**, 3108 (1998).
- [22] T. Kinoshita, T. Wenger, D. S. Weiss, *Science* **305**, 1125 (2004)
- [23] B. Paredes, A. Widera, V. Murg, O. Mandel, S. Fölling, I. Cirac, G. V. Shlyapnikov, T. W. Hansch, and I. Bloch, *Nature* **429**, 277 (2004)
- [24] M. Greiner, O. Mandel, T. Esslinger, T. Hansch, and I. Bloch, *Nature (London)* **415**, 39 (2002).
- [25] L. Onsager, *Nuovo cimento* **6**, Suppl. 2, 249 (1946).
- [26] R. P. Feynman, *Progress in Low Temperature Physics*, Vol. 1, edited by C. J. Gorter, Amsterdam, North-Holland (1955).
- [27] K. W. Madison, F. Chevy, W. Wohlleben, and J. Dalibard, *Phys. Rev. Lett.* **84**, 806, (2000).
- [28] J. R. Abo-Shaeer, C. Raman, J. M. Vogels, and W. Ketterle, *Science* **292**, 476 (2001).
- [29] P. C. Haljan, I. Coddington, P. Engels, and E. A. Cornell, *Phys. Rev. Lett.* **87**, 210403 (2001).
- [30] N. K. Wilkin, J. M. F. Gunn, and R. A. Smith, *Phys. Rev. Lett.* **80**, 2265 (1998).
- [31] N. K. Wilkin, and J. M. F. Gunn, *Phys. Rev. Lett.* **84**, 2265 (2000).
- [32] C. J. Pethick, and H. Smith, *Bose-Einstein Condensation in Dilute Gases*, Cambridge University Press, Cambridge (2002).
- [33] J. Weiner, V. S. Bagnato, S. Zilio, and P. S. Julienne, *Rev. Mod. Phys.* **71**, 1 (1999).
- [34] J. J. Sakurai, *Modern Quantum Mechanics*, (S. F. Tuan, Editor), Addison-Wesley Publishing Company (1994).
- [35] H. Feshbach, *Ann. Phys.* **19**, 287 (1962).
- [36] T. L. Ho, *Phys. Rev. Lett.* **87**, 060403 (2001).
- [37] E. J. Mueller and T. L. Ho, *Phys. Rev. Lett.* **88**, 180403 (2002).
- [38] J. Zhang, H. Zhai, *Phys. Rev. Lett.* **95**, 200403 (2005).
- [39] N. R. Cooper, E. H. Rezayi, and S. H. Simon, *Phys. Rev. Lett.* **95**, 200402 (2005).
- [40] E. A. Donley, N. R. Claussen, S. L. Cornish, J. L. Roberts, E. A. Cornell, and C. E. Wieman, *Nature* **412**, 295-299 (2001).
- [41] T. Stoferle, H. Moritz, C. Schori, M. Kohl, and T. Esslinger, *Phys. Rev. Lett.* **92**, 130403 (2004).

- [42] W. Krauth, Phys. Rev. Lett. **77**, 3695 (1996).
- [43] A. J. Leggett, Rev. Mod. Phys. **73**, 307 (2001).
- [44] R. V. E. Lovelace, and T. J. Tommila, Phys. Rev. A **35**, 3597 (1987).
- [45] G. Baym, and C. J. Pethick, Phys. Rev. Lett. **76**, 6 (1996).
- [46] A. L. Fetter, Phys. Rev. A **53**, 4245 (1996).
- [47] M. Edwards, and K. Burnett, Phys. Rev. A. **51**, 1382 (1995).
- [48] F. Dalfavo, and S. Stringari, Phys. Rev. A. **53**, 2477 (1996).
- [49] M. J. Holland, and J. Cooper, Phys. Rev. A **53**, R1954 (1996).
- [50] K. W. Madison, F. Chevy, W. Wohlleben, J. Dalibard, Phys. Rev. Lett. **84**, 806, (2000).
- [51] J. R. Abo-Shaeer, C. Raman, J. M. Vogels, and W. Ketterle, Science **292**, 476 (2001).
- [52] P. C. Haljan, I. Coddington, P. Engels, E. A. Cornell, Phys. Rev. Lett. **87**, 210403 (2001).
- [53] N. R. Cooper, Advances in Physics **57**, 539 (2008).
- [54] A. L. Fetter, Rev. Mod. Phys. **81**, 647 (2009).
- [55] P. C. Haljan, I. Coddington, P. Engels, and E. A. Cornell, Phys. Rev. Lett. **87**, 210403 (2000).
- [56] V. Bretin, S. Stock, Y. Seurin, and J. Dalibard, Phys. Rev. Lett. **92**, 050403 (2004).
- [57] V. Schweikhard, I. Coddington, P. Engels, V. P. Mogendorff, and E. A. Cornell, Phys. Rev. Lett. **92**, 040404 (2004).
- [58] M. Baranov, L. Doberk, K. Goral, L. Santos, and M. Lewenstein, Phys. Scr. T **102**, 74 (2002).
- [59] C. A. Regal, C. Ticknor, J. L. Bohn, and D. S. Jin, Phys. Rev. Lett **90**, 053201 (2003).
- [60] B. DeMarco, and D. S. Jin, Science **285**, 1703 (1999).
- [61] A. G. Truscott, K. E. Strecker, W. I. McAlexander, G. B. Partridge, and R. G. Hulet, Science **291**, 2570 (2001).
- [62] F. Schreck, L. Khaykovich, K. L. Corwin, G. Ferrari, T. Bourdel, J. Cubizolles, and C. Salomon, Phys. Rev. Lett. **87**, 080403 (2001).
- [63] K. M. O'Hara, S. L. Hemmer, M. E. Gehm, S. R. Granade, and J. E. Thomas, Science **298**, 2179 (2002).
- [64] Z. Hadzibabic, C. A. Stan, K. Dieckmann, S. Gupta, M. W. Zwierlein, A. Gorlitz, and W. Ketterle, Phys. Rev. Lett. **88**, 160401 (2002).

- [65] G. Roati, F. Riboli, G. Modugno, and M. Inguscio, Phys. Rev. Lett. **89**, 150403 (2002).
- [66] L. N. Cooper, Phys. Rev. **104**, 1189 (1956).
- [67] J. Bardeen, L. N. Cooper, J. R. Schereffer, Phys. Rev. **108**, 1175 (1957).
- [68] T. L. Ho, C. V. Ciobanu, Phys. Rev. Lett. **85**, 4648 (2000).
- [69] P. Rosenbusch, D. S. Petrov, S. Sinha, F. Chevy, V. Bretin, Y. Castin, G. Shlyapnikov, and J. Dalibard, Phys. Rev. Lett. **88**, 250403 (2002).
- [70] S. Sinha, G. V. Shlyapnikov, Phys. Rev. Lett. **94**, 150401 (2005).
- [71] P. Sanchez-Lotero, J.J. Palacios, Phys. Rev. A **72**, 043613 (2005).
- [72] A. Aftalion, X. Blanc, N. Lerner, Phys. Rev A **79**, 011603(R) (2009).
- [73] A. L. Fetter, Phys. Rev. A **75**, 013620 (2007).
- [74] N. Ghazanfari, M. O. Oktel, Eur. Phys. J. D **59**, 435 (2010).
- [75] G. B. Arfken, H. J. Weber, Mathematical Methods for Physicists (Elsevier Academic Press, 2005).
- [76] M. Linn, M. Niemeyer, A. L. Fetter, Phys. Rev. A **64**, 023602 (2001).
- [77] M. O. Oktel, Phys. Rev. A **69**, 023618 (2004).
- [78] J. G. Valatin, Proc. Roy. Soc. **238**, 132 (1956).
- [79] H. Goldstein, C. Poole. J. Safko, Classical Mechanics (Addison Wesley, 2002).
- [80] J. Friedel, Nuovo Cimento (Suppl.) 7, **287** (1958).
- [81] M. Abramowitz and I. Stegun, Handbook of Mathematical Functions, (Dover, New York, 1970).
- [82] W. H. Kleiner, L. M. Roth, and S. H. Athler, Phys. Rev. **133**, 1226(1964).
- [83] J. D. Weinstein, R. deCarvalho, J. Kim, D. Patterson, B. Friedrich, and J. M. Doyle, Phys. Rev. A **75**, 5 (1997).
- [84] A. Griesmaier, J. Werner, S. Hensler, J. Stuhler, and T. Pfau, Phys. Rev. Lett. **94**, 160401 (2005).
- [85] K. Goral, K. Rzamzewsi, and T. Pfau, Phys. Rev. A, **61**, 051601 (R)(2000).
- [86] S. Yi, and L. You, Phys. Rev. A, **63**, 053607 (2001).
- [87] L. Santos, G.V. shlyapnikov, P. Zoller, and M. Lewenstein, Phys. Rev. Lett. **85**, 9 (2000).
- [88] L. Santos, G.V. Shlyapnikov, and M. Lewenstein, Phys. Rev. Lett. **90**, 250403 (2003).
- [89] U. R. Fischer, Phys. Rev. A, **73**, 031602(R)(2006).

- [90] K. Goral, L. Santos, and M. Lewenstein, Phys. Rev. Lett. **88**, 170406 (2002).
- [91] H. P. Buchler, E. Demler, M. Lukin, A. Micheli, N. Prokofev, G. Pupillo, and P. Zoller, Phys. Rev. Lett. **98**, 060404 (2007).
- [92] M. Keceli, M. O. Oktel, Phys. Rev. A **73**, 023611 (2006).
- [93] H. Zhai, Q. Zhou, L. Rong, and L. Chang, Phys. Rev. A, **69**, 063609 (2004).
- [94] G. Baym, J. Low. Tem. Phys. **138**, 601 (2005).
- [95] A. Abrikosov, Zh. Eksp. Teor. Fiz. **32**, 1442 (1957).
- [96] J. Stenger, S. Inouye, A. P. Chikkatur, D. M. Stamper-Kurn, D. E. Pritchard, and W. Ketterle, Phys. Rev. Lett. **82**, 4569-4573 (1999).

APPENDIX A

Canonical transformation in quantum mechanics

The most important issue when dealing with quantum mechanics is how to diagonalize the Hamiltonian to obtain the eigenvalues and their corresponding eigenstates. There are number of techniques in solving problems, some with relatively easy and some with sophisticated calculations. Usually we use direct diagonalization techniques or some other like Bogoliubov transformations. However, there are some other tools that we do not use them often in quantum mechanics, one of which is the canonical transformation that connects the classical mechanics to Quantum mechanics. The interesting analogy between canonical transformation in classical mechanics with the unitary transformation in quantum mechanics is known from early life of quantum mechanics with works of (perhaps not surprisingly) Dirac. He pointed out that any transformation like $\langle q|Q\rangle$, or $\langle q|P\rangle$ between old and new canonical variables is connected with their corresponding generating functions, or more explicitly

$$\begin{aligned}\langle q|Q\rangle &= e^{\left[\frac{i}{\hbar}F_1(q,Q,t)\right]}, \\ \langle q|P\rangle &= e^{\left[\frac{i}{\hbar}F_2(q,P,t)\right]}.\end{aligned}\tag{A.1}$$

In this part, we aim to construct the connection between a canonical transformation in quantum mechanics with classical mechanics. We start by defining a linear canonical transformation in classical mechanics as follows

$$\begin{aligned}Q &= aq + bp \\ P &= cq + dp.\end{aligned}\tag{A.2}$$

The condition for canonical transformation is implied by Poisson brackets, i.e. $[Q, P] = 1$, which gives the relation

$$ad - bc = 1.\tag{A.3}$$

Since we want to construct the generating function for such transformations, we write the generating function derivatives

$$p = \frac{\partial F_1}{\partial q}, \quad P = -\frac{\partial F_1}{\partial Q}. \quad (\text{A.4})$$

To find F_1 we integrate over the first equation above, which gives us

$$F_1 = \int p dq + g(Q) \quad (\text{A.5})$$

Writing the p in terms of q , and Q from the equation system A.2 helps us progress the integration and obtain the result

$$F_1 = \frac{1}{b} \left(Qq - \frac{1}{2} a q^2 \right) + g(Q). \quad (\text{A.6})$$

The result of integration can be used in second equation A.4, in order to obtain the generating function. Finally we obtain the generating function which has the form

$$F_1 = \frac{1}{2b} [2qQ - aq^2 - dQ^2]. \quad (\text{A.7})$$

Since we know the generating function for our canonical transformation, we get back to the quantum mechanics with the same linear canonical transformations, this time obeying the well known commutation relations for position and coordinate operator. We introduce the ket $|Q\rangle$ to be the eigenstate of the Q operator. Then we try write the q -representation of a function when the Q -representation of that is known, in other words

$$\langle q|\phi\rangle = \int \langle q|Q\rangle \langle Q|\phi\rangle dQ. \quad (\text{A.8})$$

We know $\langle Q|\phi\rangle$, hence our task is now to construct $\langle q|Q\rangle$. We also know that

$$\langle q|Q|Q\rangle = Q\langle q|Q\rangle, \quad (\text{A.9})$$

and

$$\begin{aligned} \langle q|Q|Q\rangle &= \langle q|(aq + bp)|Q\rangle \\ &= aq - i\hbar b \frac{\partial}{\partial q} \langle q|Q\rangle \end{aligned} \quad (\text{A.10})$$

then equating two equations, and integrating over the new equation one can obtain

$$\langle q|Q\rangle = \varphi(Q) e^{\frac{i}{\hbar} [\frac{1}{2b}(2Qq - aq^2)]}. \quad (\text{A.11})$$

The task is now reduced to finding integral constant $\varphi(Q)$. In order to obtain it we consider a matrix element of P operator with any arbitrary state ψ

$$\begin{aligned}\langle Q|P|\psi\rangle &= \int dq \langle Q|q\rangle \langle q|P|\psi\rangle \\ &= \int dq \langle Q|q\rangle \left(cq - i\hbar d \frac{\partial}{\partial q} \right) \langle q|\psi\rangle.\end{aligned}\quad (\text{A.12})$$

We use integration by parts defining

$$\begin{aligned}u &= \langle Q|q\rangle \\ dv &= \frac{\partial}{\partial q} \langle q|\psi\rangle dq,\end{aligned}\quad (\text{A.13})$$

and since we know

$$\frac{\partial}{\partial q} \langle Q|q\rangle = -\frac{i}{\hbar} \left(\frac{Q - aq}{b} \right) \langle Q|q\rangle \quad (\text{A.14})$$

we obtain

$$\langle Q|P|\psi\rangle = \frac{d}{b} Q \langle Q|\psi\rangle + \left(c - \frac{ad}{b} \right) \int q \langle Q|q\rangle \langle q|\psi\rangle dq. \quad (\text{A.15})$$

We use the condition for the canonical transformation Eq. (A.3) to write the result as

$$\langle Q|P|\psi\rangle = \frac{d}{b} Q \langle Q|\psi\rangle - \frac{1}{b} \int q \langle Q|q\rangle \langle q|\psi\rangle dq. \quad (\text{A.16})$$

Now let us have a look at the first derivative of $\langle Q|q\rangle$ with respect to Q

$$\frac{\partial}{\partial Q} \langle Q|q\rangle = \frac{1}{\varphi^*(Q)} \langle Q|q\rangle \frac{\partial \varphi^*(Q)}{\partial Q} - \frac{iq}{b\hbar} \langle Q|q\rangle \quad (\text{A.17})$$

By extracting out the value for $-q/b \langle Q|q\rangle$ and substituting it into the integral in equation A.16 one can find

$$\langle Q|P|\psi\rangle = \left[\frac{d}{b} Q - i\hbar \frac{\partial}{\partial Q} + \frac{i\hbar}{\varphi^*(Q)} \frac{\partial \varphi^*}{\partial Q} \right] \langle Q|\psi\rangle. \quad (\text{A.18})$$

On the other hand from derivative representation of P in Q space

$$\langle Q|P|\psi\rangle = -i\hbar \frac{\partial}{\partial Q} \langle Q|\psi\rangle. \quad (\text{A.19})$$

Equations A.18, and A.19 lead us to the differential equation for $\varphi^*(Q)$, which helps us to obtain the integral constant φ as follows

$$\varphi(Q) = e^{\frac{-idQ^2}{2b}}. \quad (\text{A.20})$$

We reach the point to write $\langle q|Q\rangle$ explicitly by putting φ into equation A.11

$$\langle q|Q\rangle = e^{\frac{i}{\hbar}[\frac{1}{2b}(2qQ-aq^2-dQ^2)]}. \quad (\text{A.21})$$

This result take us to the final form of $\langle q|\phi\rangle$

$$\langle q|\phi\rangle = \int e^{\frac{i}{\hbar}[\frac{1}{2b}(2qQ-aq^2-dQ^2)]}\langle Q|\phi\rangle dQ. \quad (\text{A.22})$$

Comparing the equation for generating function F_1 , A.7 with the equation A.22 lead us to construct the important connection between the classical mechanics and quantum mechanics

$$\langle q|\phi\rangle = \int e^{\frac{i}{\hbar}F_1(q,Q,t)}\langle Q|\phi\rangle dQ. \quad (\text{A.23})$$

APPENDIX B

Wavefunctions of higher Landau levels for a particle in a rotating anisotropic harmonic trap

Since we have the ground state wavefunction, the excited states can be obtained by applying the relevant raising operators on ground state wavefunction. We give the wavefunction for six Landau level that we used in calculations during this study. (All the parameters used here are already defined in the main text.) The ground state wave function of the system is written as

$$\phi_{00} = \frac{1}{\sqrt{\pi a_x a_y}} \exp \left[-\frac{x^2}{2a_x^2} - \frac{y^2}{2a_y^2} \right] \exp \left\{ i \frac{Mxy}{\hbar} \left[\frac{\gamma}{1 + \beta_+ \beta_-} - \frac{1}{2} \left(\frac{\omega_+}{\beta_+} + \frac{\omega_-}{\beta_-} \right) \right] \right\}. \quad (\text{B.1})$$

Operator α_+ gives the excited states wave functions in each Landau level, and the other one i.e. α_- gives the higher LL states wavefunctions. The wave functions in LLL are obtained to be

$$\varphi_{m0}(x, y) = \frac{1}{\sqrt{m!}} \varphi_{00}(x, y) P_m(\xi_+) \quad (\text{B.2})$$

where

$$P_m(\xi_+) = \left(\frac{c}{2} \right)^{n/2} H_m \left(\frac{\xi_+}{\sqrt{2c}} \right) \quad (\text{B.3})$$

The wavefunctions in higher excited Landau levels also are found to be

$$\varphi_{m1}(x, y) = \frac{1}{\sqrt{m!}} \varphi_{00}(x, y) \left[\xi_- P_m(\xi_+) - 2im\rho P_{m-1}(\xi_+) \right], \quad (\text{B.4})$$

$$\begin{aligned} \varphi_{m2}(x, y) &= \frac{1}{\sqrt{2m!}} \varphi_{00}(x, y) \left\{ (\xi_-^2 - c) P_m(\xi_+) \right. \\ &\quad - 4im\rho \xi_- P_{m-1}(\xi_+) \\ &\quad \left. - 4m(m-1)\rho^2 P_{m-2}(\xi_+) \right\}, \end{aligned} \quad (\text{B.5})$$

$$\begin{aligned}
\varphi_{m3}(x, y) = & \frac{1}{\sqrt{3!m!}}\varphi_{00}(x, y)\left\{\left(\xi_-^3 - 3c\xi_- \right)P_m(\xi_+) \right. \\
& - 6im\rho\left(\xi_-^2 - c\right)P_{m-1}(\xi_+) \\
& - 12m(m-1)\rho^2\xi_-P_{m-2}(\xi_+) \\
& \left. + 8im(m-1)(m-2)\rho^3P_{m-3}(\xi_+)\right\} \tag{B.6}
\end{aligned}$$

$$\begin{aligned}
\varphi_{m4}(x, y) = & \frac{1}{\sqrt{24m!}}\varphi_{00}(x, y)\left\{\left(\xi_-^4 - 6c\xi_-^2 + 3c^2\right)P_m(\xi_+) \right. \\
& - 8mi\rho\left(\xi_-^3 - 3c\xi_- \right)P_{m-1}(\xi_+) \\
& - 24m(m-1)\rho^2\left(\xi_-^2 - c\right)P_{m-2}(\xi_+) \\
& + 32im(m-1)(m-2)\rho^3\xi_-P_{m-3}(\xi_+) \\
& \left. + 16m(m-1)(m-2)(m-3)\rho^4P_{m-4}(\xi_+)\right\} \tag{B.7}
\end{aligned}$$

$$\begin{aligned}
\varphi_{m5}(x, y) = & \frac{1}{\sqrt{120m!}}\varphi_{00}(x, y)\left\{\left(\xi_-^5 - 10c\xi_-^3 + 15c^2\xi_- \right)P_m(\xi_+) \right. \\
& - 10im\rho\left(\xi_-^4 - 6c\xi_-^2 + 3c^2\right)P_{m-1}(\xi_+) \\
& - 40m(m-1)\rho^2\left(\xi_-^3 - 3c\xi_- \right)P_{m-2}(\xi_+) \\
& + 80im(m-1)(m-2)\rho^3\left(\xi_-^2 - c\right)P_{m-3}(\xi_+) \\
& + 80m(m-1)(m-2)(m-3)\rho^4\xi_-P_{m-4}(\xi_+) \\
& \left. - 32im(m-1)(m-2)(m-3)(m-4)\rho^5P_{m-5}(\xi_+)\right\} \tag{B.8}
\end{aligned}$$

We also suggest a general form for the wavefunctions of a particle in a rotating anisotropic harmonic trap in the main text, and one can obtain the same wavefunction introduced above for any state in any Landau level using the general form

$$\varphi_{mn}(x, y) = \frac{1}{\sqrt{n!m!}}\varphi_{00}(x, y) \sum_{k=0}^n \left[(-i)^{n-k} \frac{2^{n-k}}{(n-k)!} \rho^{n-k} \frac{d^{n-k}}{d^{n-k}\xi_-} P_n(\xi_-) \frac{d^{n-k}}{d^{n-k}\xi_+} P_m(\xi_+) \right] \tag{B.9}$$

VITA

PERSONAL INFORMATION:

Nader Ghazanfari

E-mail: *gnader@newton.physics.metu.edu.tr*

Tel: 0090 312 210 43 02

EDUCATION

M.S.	METU Physics	February 2005 - August 2006
B.S.	Urmia University Physics	February 2005 - August 2006

LANGUAGES

Mother Tongue: Azeri (Azerbaijani Turkish)

Foreign Languages: English (Advanced), Turkish (Fluent), Persian (Fluent)

AWARDS

Research Award for Graduate Students: Turkish Institute for Scientific and Technological Research (TUBITAK) - Awarded March 2007

PROJECTS

The Effects of Nano-particles on Formation and Properties of High Temperature Superconductors (Supported by The Scientific and Technological Research Council of Turkey, enrolled in METU, 2006 - 2007)

ACADEMIC EXPERIENCE (Teaching Assistant)

Quantum Mechanics	January 2008 - June 2011
-------------------	--------------------------

Mathematical Methods in Physics	September 2007 - January 2008
---------------------------------	-------------------------------

RESEARCH INTERESTS

Quantum Gases; vortices in Bose-Einstein Condensates; interacting ultracold atoms

PUBLICATIONS

1. **N. Ghazanfari**, O. Oktel, Rapidly rotating fermions in anisotropic trap, European Journal of Physics D, 59, 435-441 (2010); arXiv:0910.5361v1
2. H. Sozeri, **N. Ghazanfari**, The synthesis of nanocrystalline YIG in an ammonium nitrate melt, Materials Chemistry and Physics, 113, 977-981 (2009)
3. **N. Ghazanfari**, A. Kilic, A. Gencer, H. Ozkana, Effects of Nb₂O₅ addition on superconducting properties of BSCCO, Solid State Communications, 144, 210-214 (2007)
4. H. Sozeri, **N. Ghazanfari**, Husnu Ozkan, and Ahmet Kilic, Enhancement in the high- T_c phase of BSCCO superconductors by Nb addition, SUPERCONDUCTOR SCIENCE AND TECHNOLOGY, 20, 522-528 (2007)
5. H. Sozeri, H. Ozkan, and **N. Ghazanfari**, Properties of YBCO superconductors prepared by ammonium nitrate and solid-state reaction methods, JOURNAL OF ALLOYS AND COMPOUNDS, 428, 1-7 (2007)

PUBLICATIONS-Proceedings

1. **N. Ghazanfari**, Kilic a, S. Ozcan, H. Sozen, H. Ozkan, and A. Gencer, Preparation of Nano-Scale Magnetite Fe₃O₄ and its Effects on the Bulk Bi-2223 Superconductors, CP929, Nanotechnology and Its Applications, First Sharjah International Conference, 2007 American Institute of Physics 978-0-7354-0439
2. H. Sozeri, **N. Ghazanfari**, H. Ozkan, A. Kilic, and N. Hasanli, Effect of Nb Addition on the Critical Parameters of BSCCO Superconductor, CP929, Nanotechnology and Its Applications, First Sharjah International Conference, 2007 American Institute of Physics 978-0-7354-0439